B E R I C H T E

AUS DEM

INSTITUT FÜR MEERESKUNDE

AN DER

CHRISTIAN-ALBRECHTS-UNIVERSITÄT KIEL

NR. 116

OBJECTIVE ANALYSIS OF HYDROGRAPHIC DATA SETS FROM MESOSCALE SURVEYS

VON

DOI 10.3285/IFM_BER_116

W. HILLER & R. H. KÄSE

Kopien dieser Arbeit können bezogen werden von:
Institut für Meereskunde an der Universität Kiel
Abt. Theoretische Ozeanographie
Düsternbrooker Weg 20
23/Kiel - FRG -

ISSN 0341-8561-

Abstract

The optimal interpolation techniques reviewed in this report have been illustrated with examples of their application to the "Poseidon 86" data set in order to give members of the "Warmwassersphäre"-Research Programme, who are likely to use the objective analysis program package, some insights into both practical and theoretical aspects of this estimation technique in connection with mesoscale dynamics.

The presented examples include estimation of scalar- as well as vector-fields. Special emphasis has been given to present an approach for the estimation of the statistics of the observed stochastic processes- i.e. spatial mean and covariance function- in the case where only one realisation is available.

Zusammenfassung

Anhand der Analyse des "Poseidon 86" Datensatzes werden Beispiele für die Anwendung der in diesem Bericht beschriebenen optimalen Interpolationstechnik gegeben. Ziel dabei ist es, den Mitgliedern des SFB 133 (Warmwassersphäre des Atlantiks), welche das zugehörige "Objektive Analyse"-Programmpaket benutzen wollen, einige Einblicke in sowohl praktische als auch theoretische Aspekte dieser Interpolationstechnik zu geben - soweit sie mit der Analyse mesoskaliger Prozesse zusammenhängen.

Es werden Beispiele der Schätzung sowohl von Skalar- als auch Vektorfeldern gegeben. Weiter werden die statistischen Verfahren beschrieben, welche dazu dienten, für den Fall nur einer Realisierung die räumlichen Mittelwerte und die Kovarianzfunktion der beobachteten stochastischen Prozesse zu schätzen.

CONTENTS page

1. INTRODUCTION

In the framework of the "Warmwassersphäre"-research programme of the Institut für Meereskunde hydrographic mapping experiments are being planned and carried out, requiring sampling schemes which will give information with the fewest possible station density. One is generally aiming at a proper balance between the costs of an experiment and the information gained by it, trying to avoid redundant measurements as well as having a sparse station coverage which will yield an unresolved field. Since the use of optimal estimation techniques is of common interest for several research groups, we present here a comprehensive description of the objective analysis method with emphasis on the estimation of scalar fields. The method is applied to a data set obtained during a POSEIDON cruise in the northern Canary basin (Käse & Rathlev, 1982). We will also give a brief summary of optimal vector estimation technique, discuss the assumptions involved and give an example of analysing a quasi-Eulerian velocity field derived from satellite-tracked drift buoy observations.

One of the primary objectives of the POSEIDON 86-cruise in spring 1982 was to map mesoscale density and geostrophic current fields over an area of 500 × 500 km in the Canary basin. As this experiment was designed to produce synoptic maps of mesoscale fields as well as to determine major terms in the local heat balance equation, i.e. mean advection term and divergence of the eddy flux, an accurate mapping technique was required. For the interpretation of quasi-synoptic data sets obtained from an irregularly spaced observational array, the technique of "objective analysis" has been widely used in recent years (Bretherton et al., 1976; Bretherton et al., 1980; Sarmiento, 1982, etc.).

Based on a fundamental result in estimation theory, the Gauss-Markov theorem (Liebelt, 1967), the objective analysis technique is an optimal interpolation procedure in that sense that among linear estimators on the average this one has the minimal least square error. It also yields an estimate of the residual uncertainties in the interpolated values.

As the error maps only depend on the statistics of the field, the noise level and the locations of the observational points, they can be calculated a priori for different array designs without reference to any particular data set. Thus, it is possible to minimize the expected interpolation errors provided the statistics of the field to be mapped have already been determined.

Due to the fact that our optimal estimator is linear, i.e. a weighted sum of all observations, the objective analysis procedure will produce a smoothed version of the original field with a tendency to underestimate the true field because of the specific assumptions involved in our treatment of measurement noise and small scale signals unresolved by the array.

The application of the Gauss-Markov theorem is straightforward, provided the first and second moments of the stochastic process to be estimated are known, and furthermore that the second moment matrix of all observations fulfils the condition of being positive definite. However, the determination of these moments from data can prove to be a difficult problem, especially when the joint probability function of the process varies with respect to space and

time, i.e. instationarity or inhomogeneity of the observed field. Therefore the most fundamental assumption on which the objective analysis method usually is based, is the stationarity of the statistics of the field to be mapped.

The assertion that the statistics are stationary can never be deduced from observations, because this would involve the verification that all statistic properties of the stochastic process are invariant with respect to time and space translations. It can only be postulated as a working hypothesis. Tests should be made to decide whether this assumption is significantly inconsistent with observations.

Field observations often show trends in the mean without exhibiting any form of non-stationarity of more complicated character. If there is only one realization available, this problem cannot be solved by taking the ensemble average. In this case, no progress can be made without reference to some a priori prejudice. In the present analysis of the mesoscale fields measured during "POSEIDON 86", the assumption was made that the horizontal trend in the mean can be approximated by a two-dimensional linear function fitted to the data using a multiple regression scheme. Inspection of historical data proved that a linear approximation of the mean field, which is part of the subtropical gyre, would be appropriate. The removal of a linear trend is an important step in the process of estimation of the field statistics. Otherwise, due to the fact that the observational array has finite length, neglection of the trend would in consequence redistribute power from large scales through the whole wavenumber space.

The determination of the covariance function was a major task in preparing the "POSEIDON 86" data set for objective

analysis. The historical data available for the region of interest (25°W - 18°W / 31°N - 36°N) are not sufficient to yield significant estimates for the covariances. The estimation of two-point statistics from unequally spaced data is a difficult problem (see Bretherton, 1976; Bretherton, 1980). The locations of data points were chosen more or less irregularly from a 30 × 30 nm grid (see fig. 1). As a consequence the effective alias class of unmeasurable spectral features has a more complicated structure than in the case of uniformly spaced arrays where a fixed Nyquist wave number exists. However, in practice other aspects such as logistics, synoptic decay of the field and the amount of available ship time have to be taken into account; and only if the characteristics of the wave number spectrum are known with sufficient precision a priori, an optimal efficient array can be planned which not only satisfies the requirements for synoptic mapping, but also gives sufficient information for the estimation of the covariance function or equivalently of the wave number spectrum. As this was not the case with "POSEIDON 86", our main objective was to aim at an economic sampling scheme which permits quasisynoptic mapping. On-line data processing facilities on board enabled the concentration of data point locations in dynamically interesting regions and the use of a wider and time-saving sampling scheme in regions of less activities.

Ultimately, all covariance estimation procedures are based on raw estimates of pair-wise covariances averaged over a number of realizations. Given a large ensemble of realizations, the ensemble average of the raw covariances should converge to the true covariance function. However, if only

one realization is available, the raw estimates suffer strongly from a random scatter which limits the inferences that can be drawn from them. In order to reduce the noise of the raw estimates, pairs with similar distance vector $\underset{\sim}{r}$ or $-\underset{\sim}{r}$ (assumption of stationarity) or $|\underset{\sim}{r}|$ (assumption of isotropy) were averaged. The two-dimensional spatial raw covariances derived from the "POSEIDON 86" data set seem to indicate nonisotropic features in the data and an east-west oscillation of 500 km wavelength.

An iterative nonlinear parameter fitting procedure (Gauss-Newton method) was then applied to adapt these raw covariances to one of a family of model covariance functions (METZLER et al., 1974). A similar practical approach is widely used by meteorologists ('bin method', Julian and Cline, 1974) in estimating the spectral density $E(\underset{\sim}{K})$ which under the assumption of spatial stationarity is equivalent to the specification of the spatial covariance function. (For a more detailed discussion see Bretherton and Mc Williams 1980, § 3).

As there was only one realization available, the noise inherent in the covariance raw estimates reminded us of the danger of drawing statistical inferences from too little data. Consequently the model class chosen for the final analysis was a Gaussian function which suppresses the oscillations but takes account of the nonisotropic behaviour of the raw covariances, especially of the rapid decrease of correlation in the east-west direction.

Next to the task of synoptic mapping of mesoscale fields one of the main objectives in the gathering of the "POSEIDON 86" data set was the estimation of terms in the local

temperature conservation equation. This has been described elsewhere (Käse et al., 1983), so we will only outline the procedures adopted so far as the estimation of the statistics of the observed mesoscale eddy field is concerned.

The geopotential anomaly field shown in fig. 2a reveals that three separate horizontal scales are present in the observational area. First there is the box-wide scale already mentioned that is related to the mean or gyre circulation. Second there is a smaller scale associated with a meandering flow. Third there is the mesoscale eddy field. In fig. 2b the anomaly field after removal of the linear trend is shown where a large cyclonic anomaly in the centre and an anticyclonic anomaly in the east are found due to the meandering flow. This energetic feature dominates much of the flow and property distribution and must be removed to reveal the underlying smaller scale variability, from which the eddy flux divergence is derived. Due to theoretical reasons and the observation of numerous drift buoys (fig. 13) we hypothesized the existence of a Rossby wave contribution (Käse et al., 1983). After subtraction of the spatial linear trend a simple first mode Rossby wave model

$$\psi_R(x) = P \cdot \sin(\eta y - \phi_1) \cos(\kappa x - \phi_2)$$

was fitted. The composite mean field is displayed in fig. 2c . Removal of the wave field reduces the meander-scale structure completely and reveals a mesoscale eddy field (fig. 2d). From this field raw covariances were derived and with the aid of the Gauss-Newton method adapted to one of a family of model covariance functions. In this case a Gaussian isotropic function proved to be the most suitable one.

2. OBJECTIVE ANALYSIS OF SCALAR FIELDS

The objective analysis techniques presented here have been developed for both meteorological (Gandin, 1965) and oceanographic applications (Bretherton et al., 1976; Bretherton, 1980) in the past. Ultimately, they all date back to the days of Gauss in being applications of the fundamental Gauss-Markov theorem (Liebelt, 1967). We shall give a brief summary of this technique here together with a more detailed account of the statistical and non-statistical assumptions involved.

Given a set of measurements ϕ_i of a scalar variable ψ at data points $\underset{\sim}{x}_i$, $1 \leq i \leq N$, we want to estimate ψ at the general point $\underset{\sim}{x}$ in our observational area. We assume that the measured value ϕ_i is composed of the true value $\psi(\underset{\sim}{x}_i)$ and the random noise ϵ_i

$$(1) \qquad \phi_i = \psi(\underset{\sim}{x}_i) + \epsilon_i$$

The random noise ϵ_i consists of measurement errors and small-scale fluctuations unresolved by the array (e.g. internal waves, small-scale turbulence), which we want to suppress in our analysis. We assume that the errors ϵ_i are not correlated with the field and with each other and have a known variance

$$(2) \qquad E\{\epsilon_i\} = 0$$

$$E\{\epsilon_i \epsilon_j\} = \sigma_\epsilon^2 \cdot \delta_{ij} \qquad \text{for } 1 \leq i,j \leq N$$

$$E\{\psi \epsilon_i\} = 0$$

This treatment of the noise field is rigorous and in essence correct only for the true measurement noise. However, if a small scale signal is present which is unresolved by the observational array, we assume that the scale of this noise is small compared to the scale of the observed field.

As the scale of the noise approaches zero, the noise covariance approaches a delta function of value σ_ε^2. Thus, in the limit both instrumental noise and small scale signal would become indistinguishable. In the present analysis the estimated error variance came up to 5-35 % of the total variance of the measurements depending on the depth and which property field was to be mapped horizontally.
The most general linear estimator for a scalar variable with spatially dependent mean values has the form

$$(3) \qquad \hat{\psi}(\underset{\sim}{x}) = \sum_{i=1}^{N} \alpha_{\underset{\sim}{x}i}\phi_i + \beta_{\underset{\sim}{x}}$$

Minimization of the mean square error

$$(4) \qquad \varepsilon^2(\underset{\sim}{x}) = E\{(\psi(\underset{\sim}{x}) - \hat{\psi}(\underset{\sim}{x}))^2\}$$

with respect to the coefficients $\alpha_{\underset{\sim}{x}i}$, $\beta_{\underset{\sim}{x}}$ in (3) yields

$$(5) \qquad \alpha_{\underset{\sim}{x}i} = \sum_{j=1}^{N} C_{\underset{\sim}{x}j}(A^{-1})_{ij} \quad , \quad 1 \le i \le N$$

$$\beta_{\underset{\sim}{x}} = M_{\underset{\sim}{x}} - \sum_{j=1}^{N} \alpha_{\underset{\sim}{x}j}M_j$$

where

$$(6) \qquad M_{\underset{\sim}{x}} = E\{\Psi(\underset{\sim}{x})\} \quad , \quad M_j = E\{\psi(\underset{\sim}{x}_j)\}$$

are the mean values of ψ

and

$$(7) \qquad (A)^{-1} = (C + R)^{-1}$$

is the inverse matrix of the sum of the positive definite N x N matrix of covariances

$$C_{ij} = COV\ (\psi\ (\underset{\sim}{x}_i)\ ,\ \psi\ (\underset{\sim}{x}_j)) \qquad ,\qquad 1 \leq i,j \leq N$$

of ψ at the points $\underset{\sim}{x}_i$, $\underset{\sim}{x}_j$ and the error covariance matrix

$$R_{ij} = COV\ (\varepsilon_i, \varepsilon_j) \qquad ,\qquad 1 \leq i,j \leq N$$

at points $\underset{\sim}{x}_i$, $\underset{\sim}{x}_j$.

$$(8) \qquad C_{\underset{\sim}{x},j} = COV\ (\psi\ (\underset{\sim}{x})\ ,\ \phi_j)$$

is the covariance of ψ at the interpolation point $\underset{\sim}{x}$ and the observation ϕ_j at point $\underset{\sim}{x}_j$.

Note that with the assumption of (2) the error covariance matrix reduces to a diagonal matrix with diagonal elements σ_ε^2

$$(9) \qquad R_{ij} = E\ \{\varepsilon_i \varepsilon_j\} = \sigma_\varepsilon^2 \cdot \delta_{ij} \qquad .$$

Estimates of the residual uncertainties in the interpolated values are given by the error covariance function

$$(10) \quad E\{(\psi(\underset{\sim}{x}) - \hat{\psi}(\underset{\sim}{x}))(\psi(\underset{\sim}{y}) - \hat{\psi}(\underset{\sim}{y}))\} = C_{\underset{\sim}{x}\underset{\sim}{y}} - \sum_{i=1}^{N}\sum_{j=1}^{N} C_{\underset{\sim}{x}i}\,(A^{-1})_{ij}\,C_{\underset{\sim}{y}j}$$

which yields an expected rms error

$$(11) \quad \varepsilon(\underset{\sim}{x}) = \left(C_{\underset{\sim}{x}\underset{\sim}{x}} - \sum_{i=1}^{N}\sum_{j=1}^{N} C_{\underset{\sim}{x}i}\,(A^{-1})_{ij}\,C_{\underset{\sim}{x}j}\right)^{1/2}$$

where

$$C_{\underset{\sim}{x}\underset{\sim}{y}} = \mathrm{COV}(\psi(\underset{\sim}{x}), \psi(\underset{\sim}{y})).$$

In order to account for the overall horizontal trend in the mean we assumed that the mean field can be approximated by a two-dimensional linear function which was fitted to the data by using a multiple regression scheme. Details of this fitting procedure will be discussed below.

Since the computed error maps using expression (11) cannot reflect the uncertainties inherent in the estimation of the mean of ψ, we assumed further that this error can be neglected. It should be pointed out here that - if the mean $E\{\psi(\underset{\sim}{x})\}$, the covariance function $C_{\underset{\sim}{x}\underset{\sim}{y}}$ and the noise covariance R_{ij} are known - the computation of error maps of the field to be observed is straight forward showing the ability of different sampling schemes without reference to any particular data set.

3. STATISTICAL PREPROCESSING OF SCALAR DATA SETS

3.1. ESTIMATION OF THE MEAN FIELD

Equations (3) and (5), (6) show that our optimal estimator cannot be applied without knowledge of the mean values of ψ at the observational points and the points where ψ is to be estimated.

In the analysis of the "POSEIDON 86" data set the field observations clearly show a spatial dependence in the mean fields which is basically a general meridional trend.

A practical approach to minimize the effect of the unknown mean values is to approximate the spatial mean field by a two-dimensional linear function $\hat{M}(\underset{\sim}{x})$ which is determined by a multiple regression analysis using the least squares criteria

$$(12) \qquad \sum_{i=1}^{N} (\phi_i - \hat{M}(\underset{\sim}{x}_i))^2 = \text{Min}$$

where

$$(13) \qquad \hat{M}(\underset{\sim}{x}_i) = \underset{\sim}{A} \cdot \underset{\sim}{x}_i + B \quad , \quad \underset{\sim}{A} = (A_x, A_y) \; .$$

In addition to the usual analysis of variance, an overall F-test (testing the null hypothesis that all regression parameters are zero) and partial F-tests (deletion of one regression parameter from the model) were used to check our assumptions for consistency with the data.

For the different property fields the percentage of variation explained by multiple regression was in the range of 53% - 67%. Some examples of the resulting output information for the multiple regression analysis for each property field are shown in fig. 14.

3.2. SPATIAL COVARIANCE FUNCTION

There are two main objectives which have to be accomplished when estimating the covariance functions: the first and most essential point is that every moment matrix

$$\hat{A}_{rs} = E\{\phi_r \phi_s\}$$

drawn from the estimated covariance function of ψ must be a non-negative definite matrix, i.e. none of its eigenvalues are negative. This is a characteristic of the true moment matrix

$$A_{rs} = E\{\phi_r \phi_s\}$$

on which the method to minimize the mean square error (4) in the proof of the Gauss-Markov theorem highly depends.

The second point is that the estimated covariance function approximates the true covariance function of ψ .

The standard approach chosen here to meet these two requirements was to derive raw covariances from the data and to fit a smooth curve which is a member of a class of model covariance functions and approximates the raw estimates.

Such a class of model covariances

$$(14) \qquad \mathcal{F} = \{F(\underset{\sim}{r};\underset{\sim}{P}) \ , \ \underset{\sim}{P} = (P_1,\ldots,P_l)\}$$

with the lag vector $\underset{\sim}{r} = (r_x, r_y)$ and free parameters $P_1, \ldots, P_l$ is chosen a priori together with a first guess $\hat{\underset{\sim}{P}} = (\hat{P}_1, \ldots, \hat{P}_l)$ for the undetermined parameters. A non-linear fitting procedure (METZLER et al., 1974) was used to compute an estimate $\hat{\underset{\sim}{P}}$ for the parameter vector $\underset{\sim}{P}$ which minimizes the sum of weighted squares of deviations in the values of the raw covariances and the model covariance function

$$(15) \qquad \sum_i (\hat{C}(\underset{\sim}{r}_i) - F(\underset{\sim}{r}_i, \underset{\sim}{P}))^2 \cdot w_i = \text{MIN}$$

where

$\hat{C}(\underset{\sim}{r}_i)$ is the raw covariance function (see discussion below) and W_i are appropriate weights derived from the 95 % confidence limits of the raw covariance estimates.

3.2.1. ESTIMATION OF RAW COVARIANCES

Theoretically, the estimation of raw covariances would involve the calculation of the products

$$(16) \qquad P_{ij} = (\phi_i - E\{\phi_i\})(\phi_j - E\{\phi_j\})$$

for each pair of observational points $\underset{\sim}{x}_i$, $\underset{\sim}{x}_j$ and averaging over a large number m of realizations.

$$(17) \qquad \hat{C}_{ij} = \frac{1}{m} \sum_{s=1}^{m} P_{ij}^{(s)}$$

in order to estimate the true covariance

$$(18) \qquad C_{ij} = E\{(\psi_i - E\{\psi_i\})(\psi_j - E\{\psi_j\})\}$$

between these points.

However, a different approach had to be chosen in view of the fact that only one realization was available. After subtraction of the estimated mean field (see 3.1.) from the observations, a data set with spatially quasi-stationary statistics was obtained where the covariance function was only a function of the lag vector $\underset{\sim}{r}$.

Let

$$(19) \qquad \tilde{\phi}_i = \phi_i - \hat{M}_i$$

where

$$(20) \qquad \hat{M}_i = \underset{\sim}{A} \cdot \underset{\sim}{x}_i + B$$

are estimates of the mean field given by the functional representation of the mean.

For each pair of observational points the products

$$(21) \qquad \tilde{P}(\underset{\sim}{r}) = (\tilde{\phi}_i - \hat{M})(\tilde{\phi}_j - \hat{M}) \quad , \quad \underset{\sim}{x}_j = \underset{\sim}{x}_i + \underset{\sim}{r}$$

were computed where

$$(22) \qquad \hat{M} = \frac{1}{N} \sum_{i=1}^{N} \tilde{\phi}_i$$

the sample residual mean caused by fluctuations in the anomaly field is approximately zero.

These products were averaged over all pairs of observational points in the array with an identical lag vector $\underset{\sim}{r}$ or $-\underset{\sim}{r}$

$$(23) \qquad \hat{C}\,(\underset{\sim}{r}) = \frac{1}{N} \sum_{i=1}^{m} \tilde{P}^{(i)}(\underset{\sim}{r})$$

to reduce the noise in the raw estimates (21).

Alternatively - but equivalently - these raw estimates can be computed by a generalization to two-dimensional space of the following estimators for the auto-covariance function of time series of a stationary stochastic process ψ (t) with observations ϕ (t)

$$(24) \qquad \hat{C}_{\psi}\,(r) = \frac{1}{T} \int_{o}^{T-|r|} (\phi\,(t) - \bar{\phi})\,(\phi\,(t+|r|) - \bar{\phi})\,dt$$

or

$$(25) \qquad \hat{C}'_{\psi}\,(r) = \frac{1}{T-|r|} \int_{o}^{T-|r|} (\phi\,(t) - \bar{\phi})\,(\phi\,(t+|r|) - \bar{\phi})\,dt$$

where $\bar{\phi}$ is the sample mean of ψ. Note that our estimator (23) which is equivalent to (24) is a biased estimator, whereas (25) is unbiased but has a greater mean square error than (24).

Apparently, all these estimators have intuitive appeal, i.e. they are not optimal estimators in any known sense. For example: no maximum likelihood estimator is known to exist for the autocorrelation function of an observed time series. Assuming that the probability density function is normal, the likelihood function can be derived. But the set of equations obtained by differentiation is intractable (Jenkins & Watts, 1968).

Hence, we are left with these admittedly intuitive estimators which, of course, may be compared according to criteria such as minimum mean square error or bias of the estimates.

In fig. 3a the two-dimensional raw covariances for geopotential anomaly (25/1500 dbar) are shown, whereas the corresponding confidence limits and levels of zero significance are displayed in fig. 3b,c.

As can be seen, the computed raw covariances show a considerable amount of random scatter. Inspection of the 95 % confidence limits and levels of zero significance (fig.3b,c) shows that with the present amount of data the question is left unanswered whether the east-west oscillation is primarily due to real physics or rather a result of a random sampling error inherent in the data. Even the covariances computed under the assumption of isotropy (fig. 4), with increased degrees of freedom, are not significant enough to give clear evidence concerning this point. Additionally it might be pointed out that the raw covariances are influenced by the uncertainties inherent in the approximation of the true mean field. Especially the zero crossing points are sensitive to changes in the mean field.

3.2.2. NONLINEAR FITTING OF MODEL COVARIANCES

Since only little prior information on the statistics of the mesoscale variability in the Canary basin was available, several model classes had to be tested for their ability of representing the raw covariances. The motivation for the design of the different model classes partly came from theoretical considerations, (case 4 in table 1 for instance represents a theoretical covariance function for propagating Rossby waves generated at an eastern boundary), or was implied simply because of analytic reasons (i.e. best fit to the raw covariances without systematic deviations).

Results of the nonlinear fitting procedure for the different model classes are shown in table 1, which lists the values of the weighted sum of squared deviations (WSS), correlation between the raw covariances and predicted values (COR), and parameters with 95 % confidence limits for each model function class.

In fig. 5 plots of the corresponding fitted functions are shown. Although in some cases a good fit to the data was obtained by using WSS or COR as a measure of the goodness of fit, the plots showed systematic deviations indicating a wrong model class; e.g. in case 6 for instance the covariance function does not decay fast enough leading to systematic negative correlations for large east-west separations. On the other hand, sometimes a large variability in the estimates of the parameters occured, indicating that the weighted sum of squares was not very sensitive to changes in the parameters. In these cases the model class was rejected from further analysis.

For the synoptic mapping of the data a nonisotropic Gaussian function was chosen:

$$(26) \qquad F(\underset{\sim}{r}) = e^{-\left(\frac{r_x^2}{\lambda_x^2}+\frac{r_y^2}{\lambda_y^2}\right)} \quad , \quad \lambda_x = 32.0 \ , \ \lambda_y = 48.0 \text{ nm}$$

which suppresses negative correlations.

This was motivated by the fact that even under the assumption of isotropy there was no significant negative correlation (see discussion above). As can be seen from table 1, the covariance function (26) still is a good fit to the raw covariances (table 1, case 7) and takes account of the non-isotropic features in the data, especially the rapid decrease of correlation in the east-west direction.

Some examples of the influences on the calculation of the maps using covariance functions of the remaining model classes (which represent a good fit and were not rejected) may be seen by comparing fig. 6 a) - c). The visual differences between these maps are quite noticeable but remain within the range of the predicted rms error fields.(fig. 7a)

The correlation scale in the east-west direction $\lambda_x = 32.0$ nm is comparable to the average separation between the stations of our array (fig. 1).
However, as we have not constrained our general estimator (3) to have zero bias by requiring

$$(27) \qquad \sum_{i=1}^{N} \alpha_{\underset{\sim}{x}i} = 1$$

it will give a stronger weight to the linear representation of the mean field in the regions of lower station density. As the general station coverage was good, this only happened

on the boundaries of our observational area where the predicted error variance comes up to around 50 % of the variance of the anomaly field, as can be seen from fig. 7a.

Further examples of objective mapping of different property fields based on the principles outlined so far, are displayed in fig. 15a) - d). The non-isotropic covariance function (26) was used again, with the parameters λ_x, λ_y determined from the fit of this model class to the raw covariances of the different fields. The summary of the corresponding multiple regression analysis for the mean fields is given in fig. 14.

TABLE 1

case	model class	WSS	COR	parameters nm or $(nm)^{-1}$ resp.	lower and upper confidence limits
1.	$F(\underset{\sim}{r}) = e^{-\left(\frac{r_x^2}{\lambda_x^2}+\frac{r_y^2}{\lambda_y^2}\right)} \cdot \cos(k\lvert r_x\rvert + l\lvert r_y\rvert)$	1.88	0.807	$\lambda_x = 31.7$ $\lambda_y = 47.9$ $k \approx 0$ $L \approx 0$	27.8 - 35.6 43.1 - 52.7 -0.52 - 0.52 -260.0 - 260.0
2.	$F(\underset{\sim}{r}) = e^{-\left(\frac{r_x^2}{\lambda_x^2}+\frac{r_y^2}{\lambda_y^2}\right)^{\frac{1}{2}}} \cdot (1-k\lvert r_x\rvert)$	0.667	0.91	$\lambda_x = 77.3$ $\lambda_y = 44.0$ $k = 0.151 \cdot 10^{-1}$	no estimate of error
3.	$F(\underset{\sim}{r}) = e^{-\left(\frac{r_x^2}{\lambda_x^2}+\frac{r_y^2}{\lambda_y^2}\right)} \cdot (1-k\lvert r_x\rvert)$	1.07	0.884	$\lambda_x = 99.9$ $\lambda_y = 49.0$ $k = 0.16 \cdot 10^{-1}$	92.8 - 106.9 45.6 - 52.3 $0.15 \cdot 10^{-1}$ - $0.17 \cdot 10^{-1}$
4.	$F(\underset{\sim}{r}) = e^{-\left(\frac{r_x^2}{\lambda_x^2}+\frac{r_y^2}{\lambda_y^2}\right)} \cdot \frac{\sin(k\lvert r_x\rvert)}{k\lvert r_x\rvert}$	1.87	0.807	$\lambda_x = 31.7$ $\lambda_y = 47.9$ $k = 0.5 \cdot 10^{-3}$	27.8 - 35.6 43.1 - 52.7 -252.0 - 252.0
5.	$F(\underset{\sim}{r}) = e^{-\left(\frac{\lvert r_x\rvert}{\lambda_x}+\frac{\lvert r_y\rvert}{\lambda_y}\right)} \cdot \frac{\sin(k\lvert r_x\rvert)}{k\lvert r_x\rvert}$	1.73	0.835	$\lambda_x = 69.4$ $\lambda_y = 44.8$ $k = 0.42 \cdot 10^{-1}$	39.4 - 99.3 38.6 - 51.0 $0.35 \cdot 10^{-1}$ - $0.50 \cdot 10^{-1}$

TABLE 1 (continued)

case	model class	WSS	COR	parameters nm or $(nm)^{-1}$ resp.	lower and upper confidence limits
6.	$F(\underset{\sim}{r}) = e^{-\left(\frac{\lvert r_x\rvert}{\lambda_x}+\frac{\lvert r_y\rvert}{\lambda_y}\right)}\cdot(1-k\lvert r_x\rvert)$	0.926	0.885	$\lambda_x = 91.7$ $\lambda_y = 49.4$ $k = 0.15\cdot10^{-1}$	81.7 - 101.6 44.7 - 54.2 $0.14\cdot10^{-1}$ - $0.16\cdot10^{-1}$
7.	$F(\underset{\sim}{r}) = e^{-\left(\frac{r_x^2}{\lambda_x^2}+\frac{r_y^2}{\lambda_y^2}\right)}$	1.87	0.807	$\lambda_x = 31.7$ $\lambda_y = 47.9$	28.7 - 34.5 43.1 - 52.7
8.	$F(\underset{\sim}{r}) = e^{-\left(\frac{\lvert r_x\rvert}{\lambda_x}+\frac{\lvert r_y\rvert}{\lambda_y}\right)}$	2.05	0.808	$\lambda_x = 26.7$ $\lambda_y = 45.6$	22.2 - 31.5 38.3 - 52.9
9.	$F(\lvert\underset{\sim}{r}\rvert) = e^{-\frac{(r_x^2+r_y^2)}{\lambda^2}}$	2.10	0.785	$\lambda = 37.6$	35.2 - 39.9
10.	$F(\lvert\underset{\sim}{r}\rvert) = e^{-\frac{\lvert\underset{\sim}{r}\rvert}{\lambda}}$	2.20	0.795	$\lambda = 28.9$	26.0 - 31.9

3.2.3. Statistics of the mesoscale eddy field

As mentioned already in the introduction, the process of estimating the eddy flux divergence term in the temperature conservation equation implied the problem of mapping mesoscale perturbation fields where the corresponding mean field was defined through a linear spatial trend plus Rossby wave fit.

Let

$$\phi' = \phi - (\psi_{ROSSBY} + \psi_{LIN})$$

with the composite mean field $\psi_{ROSSBY} + \psi_{LIN}$.

Again, by means of the procedures described already, raw covariances of the ϕ' field were derived based on different statistical assumptions, i.e. stationarity and/or without/ isotropy.

The two-dimensional raw correlations $\hat{C}(\underset{\sim}{r})$ for the geopotential anomaly field 25/1500 dBar are shown in fig. 9a with corresponding cross sections displayed in fig. 9b,c. Correlations derived under the assumption of isotropy are shown in fig. 10.

Our station displacement varied between 30 nm in the region of the frontal zone and $\sqrt{2} \cdot 30$ nm in the southern tranquil region where less eddy activity was observed. The raw correlations show that only under the assumption of isotropy the perturbation field is marginally correlated at 30 nm.

These raw correlations were adapted to different model correlation functions with the results as shown in table 2. In the case of a non-isotropic Gaussian function, the zonal and meridional correlation scales are identical within the 95% confidence limits. Consequently, the correlation scale λ in the two-dimensional isotropic model

function is equal to the arithmetic average of λ_x and λ_y in the non-isotropic case; the analysis of the one-dimensional isotropic raw covariances yields an identical correlation scale (case 3 of Table 2).

In case 4 and 5 of Table 2 model functions were fitted which consider the zero crossing of the isotropic raw covariances at 43 nm with subsequent negative correlations. The resulting correlation scales are larger than in case 3 (isotropic Gaussian function) where the positive form of the model function does not allow for negative correlations and - consequently - provides an underestimate of the correlation scale.

These results show that the resolution of the perturbation field was too coarse to significantly distinguish the shape of the correlation model function. The estimated correlation scales vary within the range of 20 - 38 nm depending on the assumed model function (see Table 2). Therefore, - for the final analysis - we decided to use an "a priori" function which is Gaussian, isotropic and has a correlation scale of 30 nm. Besides the fact that this function is within the significance limits consistent with our raw correlations, it enforces a separation of perturbations resolved by the box-grid and smaller sub-grid scale variability.

Our approximation of the error correlation as a delta function is only correct if the scale of the noise is infinitesimally small or at least clearly to be distinguished from the main scale of the field. Under the assumptions made with respect to the statistics of the field, this approximation is valid only if the scale of the noise is less than 15 nm.

As a consequence of the removal of the mean field the signal to noise ratio was decreased at every stage of the fitting process. The composite mean field represents about 70% of the total variability - depending on the depth level and the fact which scalar field was to be mapped -. Even under optimistic assumptions regarding the noise statistics, one finally comes up to 25% - 35% of the variance of the mesoscale perturbation field.

Having in mind future single ship experiments in this area these results underline the importance of measurement methods which can be used complementary from a ship underway - such as GEK, XCP or geostrophic velocities derived from an XBT survey through an averaged T/S relationship, which would result in a finer spatial resolution.

Based on the analysis of satellite-tracked drifting buoy observations the estimated synoptic deformation rate for the POSEIDON 86 survey was 50 km in 20 days. That means that the entire survey must be finished within that period. Consequently, additionally nested fine-scale CTD stations which are quite time consuming, prove to be no solution with respect to the statistical estimation problems encountered . This is enhanced by the fact that with the present sampling scheme every station is statistically independent because of the short correlation scale of 30 nm or less. Thus, several nested fine-scale CTD-stations would have to be implemented in the survey pattern at dynamically similar regions so to have enough mesoscale events with sufficient degrees of freedom. This is hard to achieve without prior information about the flow field.

The above remarks are valid for the case that only one realization is available. If there are several realizations for the same observational area with similar dynamics involved, the covariance

fitting approach used here can be replaced by the more refined spectral model fitting approach as described by Bretherton et al. (1980). Their estimator is optimally efficient in the sense that no other unbiased linear estimator operating on the same subspace of spectral features, can have less uncertainties. The more precise estimation of the underlying statistics which - in consequence - improves the accuracy of reproducing the true flow or property field, must be complemented by an array design considering the expected or known spectal features. One of the fundamental properties of an irregular array is the intrinsic alias class, which is the set of spectral features for which - regardless of the number of realizations - no information can be obtained or power between adjacent wave numbers discriminated through observations. Several examples of optimal array design for isotropic or non-isotropic stochastic processes are given by Bretherton & McWilliams (1979) based on the maximization of information gained according to standard theory (Middleton, 1960). If the array is intended to serve synoptic mapping purposes as well, a more uniform distribution in space is desirable. For example, a rhombic two-dimensional array as described by Petersen & Middleton (1962) is optimal for a band-limited isotropic process.

Table 2

Case	model class	WSS	COR	parameters (nm)	lower and upper 95% confidence limits
1.	$F(\underset{\sim}{r}) = e^{-\left(\frac{r_x^2}{\lambda_x^2} + \frac{r_y^2}{\lambda_y^2}\right)}$	0.93	0.77	$\lambda_x = 20.3$ $\lambda_y = 23.1$	17.5 - 23.0 20.5 - 25.6
2.	$F(\lvert\underset{\sim}{r}\rvert) = e^{-\frac{\lvert r\rvert^2}{\lambda^2}}$	0.94	0.77	$\lambda = 21.7$	19.9 - 23.4
	1-dimensional isotropic raw correlations:				
3.	$F(\lvert\underset{\sim}{r}\rvert) = e^{-\frac{\lvert r\rvert^2}{\lambda^2}}$	0.54	.981	$\lambda = 21.7$	19.9 - 23.5
4.	$F(\lvert\underset{\sim}{r}\rvert) = (1-k^2\cdot\lvert\underset{\sim}{r}\rvert^2)e^{-\frac{\lvert r\rvert^2}{\lambda^2}}$	.037	.985	$\lambda = 35.7$ $k = .25\cdot10^{-1}$	33.8 - 37.7 $.245\cdot10^{-1}$ — $.268\cdot10^{-1}$
5.	$F(\lvert\underset{\sim}{r}\rvert) = (1-k\cdot\lvert\underset{\sim}{r}\rvert)e^{-\frac{\lvert r\rvert}{\lambda}}$	.031	.987	$\lambda = 28.6$ $k = .22\cdot10^{-1}$	25.8 - 31.4 $.200\cdot10^{-1}$ — $.242\cdot10^{-1}$

4. Objective Analysis of vector fields

In this section we shall give a brief summary of the adaption of the basic algorithm to vector fields (Bretherton et al., 1976). Some preliminary remarks will serve as an introduction to the problems which will arise.

Given a set of observations of a horizontal velocity field at N points

$$\underset{\sim}{u}(\underset{\sim}{x}_i) = (u_1(\underset{\sim}{x}_i), u_2(\underset{\sim}{x}_i)) \qquad 1 \le i \le N \tag{28}$$

we can straightforward adapt the basic algorithm by introducing the observation vector

$$\underset{\sim}{\phi} = (\phi_1,\ldots,\phi_{2N}) = (u_1(\underset{\sim}{x}_1),\ldots,u_1(\underset{\sim}{x}_N),u_2(\underset{\sim}{x}_1),\ldots,u_2(\underset{\sim}{x}_N)) \tag{29}$$

For brevity we assume that the velocity field has zero mean. With the aid of the general linear estimator (3), we obtain optimal estimates of the velocity components at a general point $\underset{\sim}{x}$ in the observational area

$$\begin{cases} \hat{u}_1(\underset{\sim}{x}) = \sum_{j=1}^{2N} C^{(1)}_{\underset{\sim}{x}j} \sum_{i=1}^{2N} A^{-1}_{ji}\,\phi_i \\ \hat{u}_2(\underset{\sim}{x}) = \sum_{j=1}^{2N} C^{(2)}_{\underset{\sim}{x}j} \sum_{i=1}^{2N} A^{-1}_{ji}\,\phi_i \end{cases} \tag{30}$$

where

$$C_{\underset{\sim}{x}j}^{(\ell)} = E\{u_\ell(\underset{\sim}{x})\, u_1(\underset{\sim}{x}_j)\} \quad \text{for} \quad \begin{matrix} 1 \le j \le N \\ 1 \le \ell \le 2 \end{matrix}$$

(31) and $C_{\underset{\sim}{x}j}^{(\ell)} = E\{u_\ell(\underset{\sim}{x})\, u_2(\underset{\sim}{x}_j)\} \quad \text{for} \quad N+1 \le j \le 2N$

are the covariances of the ℓ^{th} velocity component to be estimated and the j^{th} observation and

(32) $$A_{ij} = E\{\phi_i \phi_j\} \qquad 1 \le i,j \le 2N$$

is the covariance between all pairs of observations. The error in the velocity estimates is given by the general Gauß-Markov theorem in the following way. First, we introduce the 2×2 error matrix C_ε

$$C_\varepsilon = E\{\underset{\sim}{e}^T \cdot \underset{\sim}{e}\} = \begin{pmatrix} E\{e_1 e_1\} & , & E\{e_1 e_2\} \\ E\{e_2 e_1\} & , & E\{e_2 e_2\} \end{pmatrix}$$

where

$$\underset{\sim}{e} = (e_1, e_2) = \hat{\underset{\sim}{u}} - \underset{\sim}{u} = (\hat{u}_1 - u_1 \; , \; \hat{u}_2 - u_2)$$

where $\underset{\sim}{u}$ is the true velocity and $\hat{\underset{\sim}{u}}$ the estimate.

According to the Gauß-Markov theorem, the trace of C_ε is minimal for our optimal estimate (30):

$$E\{|\underset{\sim}{e}|^2\} = E\{e_1^2\} + E\{e_2^2\} = tr\,(C_\varepsilon) = MIN$$

Thus, we can specify the root-mean-square error ε of the estimate $\hat{\underset{\sim}{u}}(\underset{\sim}{x})$:

$$\varepsilon = E\{|\underset{\sim}{e}|^2\}^{\frac{1}{2}} = E\{|\hat{\underset{\sim}{u}}-\underset{\sim}{u}|^2\}^{\frac{1}{2}}$$

$$= \left(\sum_{\ell=1}^{2} C^{(\ell)}_{\underset{\sim}{x}\underset{\sim}{x}} - \sum_{\ell=1}^{2} \sum_{i,j=1}^{2N} C^{(\ell)}_{\underset{\sim}{x}i} \, (A^{-1})_{ij} \, C^{(\ell)}_{\underset{\sim}{x}j} \right)^{\frac{1}{2}} \tag{33}$$

where

$$C^{(\ell)}_{\underset{\sim}{x}\underset{\sim}{x}} = E\{u_\ell(\underset{\sim}{x}) \, u_\ell(\underset{\sim}{x})\} \qquad \text{for} \quad 1 \le \ell \le 2$$

is the variance of the ℓ^{th} velocity component.

If we consider the velocity components as stochastic functions and assume that their joint probability function is independent of arbitrary spatial translations, i.e. homogeneity, and if we assume further that the standard assumption (2) holds, i.e. the errors inherent in the velocity measurements are not correlated with the velocity field and with each other and have a known variance E, we can rewrite (32) in terms of the velocity correlation tensor $R_{k\ell}(r)=E\{u_k(\underset{\sim}{x})u_\ell(\underset{\sim}{x}+\underset{\sim}{r})\}$:

$$A_{i,j} = R_{11}(\underset{\sim}{r}_{ij}) + E\,\delta_{ij} \qquad , \qquad 1 \le i,j \le N \tag{34}$$

$$A_{i,j+N} = R_{12}(\underset{\sim}{r}_{ij})$$

$$A_{i+N,j} = R_{21}(\underset{\sim}{r}_{ij})$$

$$A_{i+N,j+N} = R_{22}(\underset{\sim}{r}_{ij}) + E\,\delta_{ij}$$

with

$$\underset{\sim}{r}_{ij} = \underset{\sim}{x}_i - \underset{\sim}{x}_j$$

Thus, we are left with the problem of specifying the velocity correlation tensor.

In order to give a simple mathematical description of $R_{k\ell}(\underset{\sim}{r})$, we will

adopt the standard approach used elsewhere (Bretherton et al., 1976; McWilliams, 1976), and assume that the velocity field is isotropic. Modified for a 2-dim.velocity field, this means that the probability distribution is invariant under arbitrary rotations about a vertical axis and reflections in any direction. The velocity correlation $R_{k\ell}(\underset{\sim}{r})$ is then an isotropic second-order two point tensor and, therefore, has the form (Bachelor, 1959)

$$(35) \qquad R_{k\ell}(\underset{\sim}{r}) = A(r)\, r_k\, r_\ell + B(r)\, \delta_{k\ell} \quad , \quad \text{where} \quad r = |\underset{\sim}{r}|$$

where A, B are even scalar functions of r. (It should be noted that since the beginning of this chapter, we are ignoring time-dependence.)

As our main interest concentrates on the interpretation of mesoscale velocity measurements, this - we admit - is a poor assumption which will scarcely be fulfilled in real physics. However, it should be borne in mind that under the least restrictive symmetry condition symmetry about a plane, $R_{k\ell}(\underset{\sim}{r})$ is the sum of 35 terms including vector arguments (Batchelor, 1959).

The condition of homogeneity has ensured that

$$R_{k\ell}(\underset{\sim}{r}) = R_{\ell k}(-\underset{\sim}{r})$$

the condition of isotropy makes $R_{k\ell}(\underset{\sim}{r})$ fully symmetrical in the two suffixes:

$$R_{k\ell}(\underset{\sim}{r}) = R_{\ell k}(\underset{\sim}{r})$$

The continuity condition

$$\nabla \cdot \underset{\sim}{u} = 0$$

has further consequences for $R_{k\ell}(\underset{\sim}{r})$ (summation convention for the tensor suffixes is used from now on until the end of this chapter):

$$\frac{\partial}{\partial r_\ell} u_\ell \ (\underset{\sim}{x}+\underset{\sim}{r}) = 0$$

which yields for fixed k:

$$E \{u_k(x) \frac{\partial}{\partial r_\ell} u_\ell \ (\underset{\sim}{x}+\underset{\sim}{r})\} = \frac{\partial}{\partial r_\ell} (E \{u_k(x) \ u_\ell \ (\underset{\sim}{x}+\underset{\sim}{r})\})$$

$$= \frac{\partial}{\partial r_\ell} R_{k\ell}(r) = 0$$

With the form of $R_{k\ell}(\underset{\sim}{r})$ established by (35), it follows

$$(36) \qquad 3A(r) + r \frac{\partial A(r)}{\partial r} + \frac{1}{r} \frac{\partial}{\partial r} B(r) = 0$$

Introduction of the convenient longitudinal and transversal velocity correlation functions

$$f(r) = \frac{E \{u_{\|}(\underset{\sim}{x}) \ u_{\|}(\underset{\sim}{x}+\underset{\sim}{r})\}}{E \{u_{\|}^2\}}$$

$$g(r) = \frac{E \{u_{\perp}(x) \ u_{\perp}(\underset{\sim}{x}+\underset{\sim}{r})\}}{E \{u_{\perp}^2\}}$$

for two points $\underset{\sim}{x}$, $\underset{\sim}{x} + \underset{\sim}{r}$ at distance r apart, gives the following relations to the scalar functions A(r), B(r) of (35)

$$
\begin{aligned}
F(r) &= u^2 f(r) = E\{u_{\parallel}(\underset{\sim}{x})\, u_{\parallel}(\underset{\sim}{x}+\underset{\sim}{r})\} = r^2 A(r) + B(r) \\
G(r) &= u^2 g(r) = E\{u_{\perp}(\underset{\sim}{x})\, u_{\perp}(\underset{\sim}{x}+\underset{\sim}{r})\} = B(r)
\end{aligned} \tag{37}
$$

where $F(r)$, $G(r)$ are the longitudinal and transversal covariance functions respectively, and

$$u^2 = E\{u_{\parallel}^2\} = E\{u_{\perp}^2\} = E\{u_k^2\} \tag{38}$$

is the total variance of the velocity field which equals the component variance $E\{u_k^2\}$ because of the isotropy assumption.

In the derivation of (36), we made use of the transformation

$$
\begin{aligned}
u_{\parallel} &= \cos\alpha \cdot u_1 + \sin\alpha \cdot u_2 \\
u_{\perp} &= -\sin\alpha \cdot u_1 + \cos\alpha \cdot u_2
\end{aligned}
$$

where α is the angle between $\underset{\sim}{r}$ and the x_1-axis. Without limitations to the general case, $\underset{\sim}{r}$ may be assumed to be positioned in the (x_1, x_2) plane as a consequence of the isotropy assumption.

From (37) it follows that

$$
\begin{aligned}
A(r) &= \frac{1}{r^2}\,(F(r) - G(r)) \\
B(r) &= G(r)
\end{aligned} \tag{39}
$$

Thus, we can rewrite $R_{k\ell}(\underset{\sim}{r})$ in terms of $F(r)$ and $G(r)$

$$R_{k\ell}(\underset{\sim}{r}) = (F(r) - G(r)) \cdot \frac{r_k r_\ell}{r^2} + G(r) \cdot \delta_{k\ell} \tag{40}$$

From (36) and (39) it follows that, in fact, we have to determine only F(r)and its first derivative:

$$(41) \qquad G(r) = F(r) + r \cdot \frac{\partial}{\partial r} F(r)$$

Thus, for our original problem of mapping a two-dimensional horizontal velocity field, we can specify the correlation tensor used in (39) in terms of F(r) and F'(r):

$$R_{11}(\underset{\sim}{r}) = F(r) + \frac{r_2^2}{r} \cdot F'(r)$$

$$(42) \qquad R_{12}(\underset{\sim}{r}) = R_{21}(\underset{\sim}{r}) = -\frac{r_1 r_2}{r} \cdot F'(r)$$

$$R_{22}(\underset{\sim}{r}) = F(r) + \frac{r_1^2}{r} \cdot F'(r)$$

where $F'(r) = \frac{\partial}{\partial r} F(r)$

If the velocity field is known to be non-divergent, or if non-divergence is raised to be an axiom of the analysis, (i.e. if a geostrophic view of a measured velocity field is desired or if low frequency currents are analysed which are in approximate geostrophic balance,) it is convenient to introduce a stream function $\psi(\underset{\sim}{x})$ with

$$u_1(\underset{\sim}{x}) = -\frac{\partial \psi(\underset{\sim}{x})}{\partial x_2} \quad , \quad u_2(x) = \frac{\partial \psi(\underset{\sim}{x})}{\partial x_1}$$

and covariance function

$$C(\underset{\sim}{r}) = E\{\psi(\underset{\sim}{x})\ \psi(\underset{\sim}{x}+\underset{\sim}{r})\}$$

From non-divergence and with the aid of (41), we obtain the following relations between C(r), F(r) and G(r)

$$F(r) = -\frac{1}{r}\frac{\partial}{\partial r} C(r)$$

(43)

$$G(r) = \frac{\partial}{\partial r}(r \cdot F(r)) = -\frac{\partial^2 C(r)}{\partial r^2}$$

As pointed out by Bretherton et al., 1976, a direct consequence of the use of statistics consistent with horizontal non-divergence, is the fact that the divergence of the estimated field will vanish - regardless of the nature of the measurements. This can be seen by taking the divergence of the velocity estimates (30). With weights

$$\alpha_j = \sum_{i=1}^{N} (A^{-1})_{ji} \phi_i \qquad (44)$$

and

$$\alpha_{j+N} = \sum_{i=N+1}^{2N} (A^{-1})_{ji} \phi_i$$

we obtain

$$\frac{\partial \hat{u}_1(\underset{\sim}{x})}{\partial x_1} + \frac{\partial \hat{u}_2(\underset{\sim}{x})}{\partial x_2} = \frac{\partial}{\partial x_1}\left(\sum_{j=1}^{N} E\{u_1(\underset{\sim}{x})u_1(\underset{\sim}{x}_j)\}\cdot\alpha_j + \sum_{j=1}^{N} E\{u_1(\underset{\sim}{x})u_2(\underset{\sim}{x}_j)\}\cdot\alpha_{j+N}\right. \qquad (45)$$

$$\left. + \frac{\partial}{\partial x_2}\left(\sum_{j=1}^{N} E\{u_2(\underset{\sim}{x})u_1(\underset{\sim}{x}_j)\}\cdot\alpha_j + \sum_{j=1}^{1} E\{u_2(\underset{\sim}{x})u_2(\underset{\sim}{x}_j)\}\cdot\alpha_{j+1}\right.\right.$$

$$= \sum_{j=1}^{N} \left(\frac{\partial}{\partial x_1} E\{u_1(\underset{\sim}{x})\phi_j\} + \frac{\partial}{\partial x_2} E\{u_2(\underset{\sim}{x})\phi_j\}\right)\cdot a_j$$

$$+ \sum_{j=1}^{N} \left(\frac{\partial}{\partial x_1} E\{u_1(\underset{\sim}{x})\phi_{j+N}\} + \frac{\partial}{\partial x_2} E\{u_2(\underset{\sim}{x})\phi_{j+N}\}\right)\cdot a_{j+N}$$

$$= \sum_{j=1}^{2N} E\left\{\left(\frac{\partial}{\partial x_1} u_1(\underset{\sim}{x}) + \frac{\partial}{\partial x_2} u_2(\underset{\sim}{x})\right)\phi_j\right\}\cdot a_j = 0 \quad .$$

Thus, once the a priori constraint of non-divergence has been applied by selecting statistics consistent with a non-divergent field, the estimated field will be non-divergent even if the data base shows marked inconsistencies with that assumption.

Consequently, if theoretical reasons imply - for example - that in the observational area the importance of the non-linear and frictional terms in the equation of motion is small compared to the influence of the Coriolis term , a geostrophic approximation may significantly improve the estimated velocity field, especially when associated with mesoscale motion. On the other hand, the example of vector analysis given below, i.e. estimation of a quasi-Eulerian velocity field from averaged and low-pass filtered drifting buoy observations, in some cases displayed marked differences between the estimated non-divergent velocity field and the observational field in space, showing that the assumption of non-divergence was clearly not applicable.

Finally, as an alternative possibility of mapping a non-divergent velocity field, we will present the modification of the basic algorithm for estimating the stream function itself.

According to Bretherton et al. , 1976, the basic estimation algorithm for operationally derived fields, obtained by application of a linear differential or integral operator

$$\mathcal{L}_{\underset{\sim}{x}}(\psi)$$

to the field ψ which is measured, is affected by the operator $\mathcal{L}_{\underset{\sim}{x}}$ in the following way: First,the weights α_j derived from the observations by (44) used to estimate $\psi_{\underset{\sim}{x}}$, are the same as those used to estimate $\mathcal{L}_{\underset{\sim}{x}}(\psi)$. Second, the covariance

$$C_{\underset{\sim}{x}j} = E\{\psi_{\underset{\sim}{x}}\phi_j\}$$ used to estimate $\psi_{\underset{\sim}{x}}$ changes to

$$L_{\underset{\sim}{x}j} = E\{\mathcal{L}_{\underset{\sim}{x}}(\psi)\phi_j\}$$

An important direct consequence from this fact is

$$(46) \qquad \mathcal{L}_{\underset{\sim}{x}}(\hat{\psi}) = \mathcal{L}_{\underset{\sim}{x}}\left(\sum_{j=1}^{N} E\{\psi_{\underset{\sim}{x}}\phi_j\}\,\alpha_j\right)$$

$$= \sum_{j=1}^{N} E\{\mathcal{L}_{\underset{\sim}{x}}(\psi)\phi_j\}\,\alpha_j = \hat{\mathcal{L}}_{\underset{\sim}{x}}(\psi)$$

i.e. the linear operation $\mathcal{L}_{\underset{\sim}{x}}$ on the optimal estimate $\hat{\psi}_{\underset{\sim}{x}}$ is equal to the optimal estimate of $\mathcal{L}_{\underset{\sim}{x}}(\psi)$ itself.

For the stream function $\psi(\underset{\sim}{x})$ this means

$$(47) \qquad \hat{\psi}(\underset{\sim}{x}) = \sum_{j=1}^{2N} L_{\underset{\sim}{x}j} \sum_{i=1}^{2} (A^{-1})_{ji} \phi_i$$

with the observational vector $\underset{\sim}{\phi}$ defined by (29) and covariances

$$L_{\underset{\sim}{x}j} = E\{\psi(\underset{\sim}{x})\, u_1(\underset{\sim}{x}_j)\} \qquad \text{for} \quad 1 \le j \le N$$

and

$$L_{\underset{\sim}{x}j} = E\{\psi(\underset{\sim}{x})\, u_2(\underset{\sim}{x}_j)\} \qquad \text{for} \quad N+1 \le j \le 2N\ .$$

The root mean-square error in the estimate $\hat{\psi}(\underset{\sim}{x})$ is defined by

$$(48) \qquad \varepsilon(\underset{\sim}{x}) = (L_{\underset{\sim}{x}\underset{\sim}{x}} - \sum_{i,j=1}^{2N} L_{\underset{\sim}{x}i}\, (A^{-1})_{ij}\, L_{\underset{\sim}{x}j})^{\frac{1}{2}}$$

where

$$L_{\underset{\sim}{x}\underset{\sim}{x}} = E\{\psi(\underset{\sim}{x})\, \psi(\underset{\sim}{x})\} \qquad \text{is the variance of } \psi.$$

Under the assumption of isotropy and non-divergence, the covariances $L_{\underset{\sim}{x}j}$ can be derived from the covariance of the stream function C(r)

$$(49) \qquad \frac{\partial}{\partial r_2} C(r) = E\{\psi(\underset{\sim}{x})\, u_1(\underset{\sim}{x}+\underset{\sim}{r})\} = -\frac{r_2}{r} \frac{\partial}{\partial r} C(r)$$

$$\frac{\partial}{\partial r_1} C(r) = E\{\psi(\underset{\sim}{x})\, u_2(\underset{\sim}{x}+\underset{\sim}{r})\} = \frac{r_1}{r} \frac{\partial}{\partial r} C(r)$$

With the aid of (43), it follows that

$$(50) \qquad L_{\underset{\sim}{x}j} = r_2 \cdot F(r) \qquad \text{for} \quad 1 \le j \le N$$

and

$$L_{\underset{\sim}{x}j} = - r_1 \cdot F(r) \qquad \text{for} \quad N+1 \le j \le 2N$$

At the beginning of this section, we made the asumption that the velocity field has zero mean. In case of spatial stationarity and non-zero mean, the component mean values can be evaluated and removed at the outset of the analysis. After estimation of the velocity field, the mean values are added at every grid point.

When we want to estimate the stream function field $\psi(\underset{\sim}{x})$ with non-zero mean $E\{\psi(\underset{\sim}{x})\}$, the input velocity vector mean $E\{\underset{\sim}{u}\} = (\bar{u},\bar{v})$ is first removed. Within the extent of accuracy to which the observed velocity field obeys the non-divergence requirements, $-\bar{u}$ and $\bar{v}$ represent the meridonal or zonal gradients of $E\{\psi(\underset{\sim}{x})\}$ respectively. The total estimated stream function field can thus be approximated in the following way:

$$(51) \qquad \hat{\psi}(\underset{\sim}{x}) = \hat{\psi}'(\underset{\sim}{x}) + (\bar{v} \cdot x - \bar{u} \cdot y) + \psi_o$$

where $\psi_0 = \psi\,(0,0)$ is an unknown additive constant.

4.1. Analysis of quasi-Eulerian velocity fields

As an example of vector analysis, we will describe the estimation of quasi-Eulerian velocity fields derived from drifting buoy trajectories.

Prior to the 1982 density survey by R.V. "Poseidon" a set of four satellite-tracked drifting buoys was launched in the observational area of the Canary Basin (Fig. 1) by R.V. "Meteor". Together with two previously launched drifting buoys entering the box area from the north, a total of six drifters was observed during 1982 yeardays 70 - 100 in the region of Madeira and the Azore Islands. They are a subset of 68 drifting buoys released during 1981 / 1982 by the Institut für Meereskunde in Kiel within a long-term experiment. Object of this experiment is to investigate mean currents and eddy activity in the north-east Atlantic (Krauss & Käse, 1983).

Using a finite difference scheme, the trajectories were transformed to quasi-Eulerian velocity time series. The latter were low-pass filtered so to remove all oscillations shorter or equal to the inertial period. Daily averages were computed to serve as data base for the objective analysis. From these averages the input vector field was chosen by selecting velocity values every five days for each drifter, assuming that - due to the mean displacement of about 30 km within five days - the input velocity field is dominantly correlated only as a function of spatial separation.

As the covariance function for the stream function we use the same model function as derived from the analysis of the surface geopotential anomaly field (see chapter 3.2) because information obtained from only six drifting buoys did not allow a statistically significant estimation of both the longitudinal and the transversal covariance function.

With the longitudinal integral scale defined by

$$L_{\parallel} = \int_0^{\infty} f(r)\, dr \qquad \text{(Batchelor, 1959)}$$

and the isotropic correlation scale λ estimated to be 75 km (see Table 1, case 7), we obtain

$$L_{\parallel} = \frac{1}{2}\sqrt{\pi}\,\lambda = 64 \text{ km}$$

which is consistent with the estimate of the longitudinal integral scale as derived from the analysis made of the original data set of all drifters in that region (Krauss & Käse, 1983).

We use the following system of functions

$$C(r) = B' \cdot e^{-\frac{r^2}{\lambda^2}}$$

$$F(r) = (2 \cdot B'/\lambda^2) \cdot e^{-\frac{r^2}{\lambda^2}}$$

$$G(r) = (2 \cdot B'/\lambda y) \cdot [1 - 2r^2/\lambda^2] \cdot e^{-\frac{r^2}{\lambda^2}}$$

where $B = VAR(\underset{\sim}{u}) = 2B'/\lambda^2$

and $B' = VAR(\psi)$.

The estimated velocity field is shown in fig. 13a together with the input vector field. The error variance within the dotted area exceeds 50% of the variance of the total field.

Due to the sparse spatial coverage of the input vector field - as derived from the Lagrangian float trajectories - the region where the expected error variance is less than 50 % of the total variance is small and patchy. North of 36°N there is no reliable velocity estimate except the small error island at 36.5 N, 23.5 W at the location of one data point.

In Fig. 13b) we have analysed the same input velocity field under the assumption that the isotropic correlation scale is 200 km. The error variance is assumed to be 30 % of the variance of the total field. This is about the same value as was deduced from the Rossby wave fit to the geostrophic velocity field, where the composite mean field was analysed to represent 70 % of the total variability. This means that we have treated mesoscale variability on scales smaller than 200 km essentially as noise. The smoothed estimated velocity field thus represents only scales of the composite mean field, with the Rossby wave clearly apparent as an alternating sequence of cyclonic and anticyclonic eddies.

Due to the sparsity of data points these results should be interpreted qualitatively only, as the amount of "a priori" constraints imposed on the data in the form of the isotropic nondivergent statistics, assumed correlation scale and noise level is considerable.

5. DISCUSSION

The optimal interpolation techniques reviewed in this report have been illustrated with examples of their application to the "Poseidon 86" data set in order to give members of the "Warmwassersphäre"-Research Programme who are likely to use the objective analysis program package, some insights into both practical and theoretical aspects of this estimation technique.

As has been demonstrated by several other investigators and research groups in recent years (see reference list), this theory is powerful and practical as well and provides an optimal linear minimum mean square error estimate of the observed variable fields.

One of the important features of this theory is the fact that it may be applied equally well to estimation problems in time and space even if the joint probability density function of the random variables observed is unknown, ie. our estimate is "distribution free". Based upon the first and second moments of the stochastic process under consideration, an optimal estimate is derived provided the second moment matrix of the observations is non-singular. Thus - at least in principle - it should be possible to treat instationary phenomena as well. However, the determination of these moments from data might turn out to be a difficult problem having in mind that the second moment matrix of all observations is almost certainly singular. Therefore, the objective analysis method usually is based upon the assumption of spatial stationarity of the field to be mapped.

The first and second moments are then derived from the known or assumed mean and covariance function which in case of a Gaussian process determines all statistical properties of the process.

By this approach the question of the quality of the estimation or better of the reproduction of the true flow or property field is reduced to the question of how accurately the underlying statistics of the field can be estimated.

The problems encountered in the statistical analysis of the "Poseidon 86" data set have been discussed in detail in this report. Reference is thus made to the reader to the different chapters and the introductory remarks so to be able to understand the limitations of this approach. The most critical point in the present analysis was the fact that the result in adapting the model correlation functions to the raw correlations is - to a large extent - determined by the shape of the model function itself. This must be attributed to the fact that by the synoptic error and unresolved small scale signals the tuning of the model function is limited to only a small number of parameters.

The authors had the feeling that with the present amount of data and error sources a more refined spectral fitting approach - as for example described by Bretherton & McWilliams,1980, - would not be appropriate. However, if we have more than one realization of the same processes available, a more refined fitting of the spectral features encountered may significantly improve the accuarcy when reproducing the true field.

REFERENCES

BRETHERTON, F.P., R.E. DAVIS & C.B. FANDRY, 1976: A technique for objective analysis and design of oceanographic experiments applied to MODE-73. Deep-Sea Res., 23, 559-582

BRETHERTON, F.P. & J.C. McWILLIAMS, 1980: Estimations from irregular arrays. Rev. Geophys. and Space Phys., 18, 4, 789-812

BRETHERTON, F.P. & J.C. McWILLIAMS, 1979: Spectral estimation from irregular arrays. Techn. Note NCAR/TN-138+STR, National Center for Atmospheric Research, Boulder/Colorado

GANDIN, L.S., 1965: Objective analysis of meteorological fields. Israel Program for scientific translations

JENKINS, G.M. & D.G. WATTS, 1968: Spectral analysis and its application. Holden-Day

JULIAN, P.R. & A.K. CLINE, 1974: The direct estimation of spatial wave-number spectra of atmospheric variables. J. Atmosph. Sci., 31, 1526-1539

KÄSE, R.H., T. SANFORD, W. ZENK & W. HILLER, 1983: Currents, fronts and eddy fluxes in the Canary Basin. (submitted for publication)

KRAUSS, W. & R.H. KÄSE, 1983: Mean circulation and eddy kinetic energy in the eastern North Atlantic (submitted for publication).

LIEBELT, P.B., 1967: An introduction to optimal estimation. Addison-Wesley

METZLER, C.M., G.L. ELFRING & A.J. McEWEN, 1974: A package of computer programs for pharmacokinetic modeling. Biometrics, pp. 562

MIDDLETON, D., 1960: An introduction to statistical communication theory. McGraw-Hill, New York

PETERSEN, D.P. & D. MIDDLETON, 1962: Sampling and reconstruction of wave number limited functions in N-dimensional spaces. Inf. and Control, 5, pp. 279

SARMIENTO, J.L., J. WILLEBRAND & S. HELLERMANN, 1982: Objective analysis of Tritium observations in the Atlantic Ocean during 1971-74. Ocean Tracers Lab. Technical Report No. 1, Princeton University, New Jersey

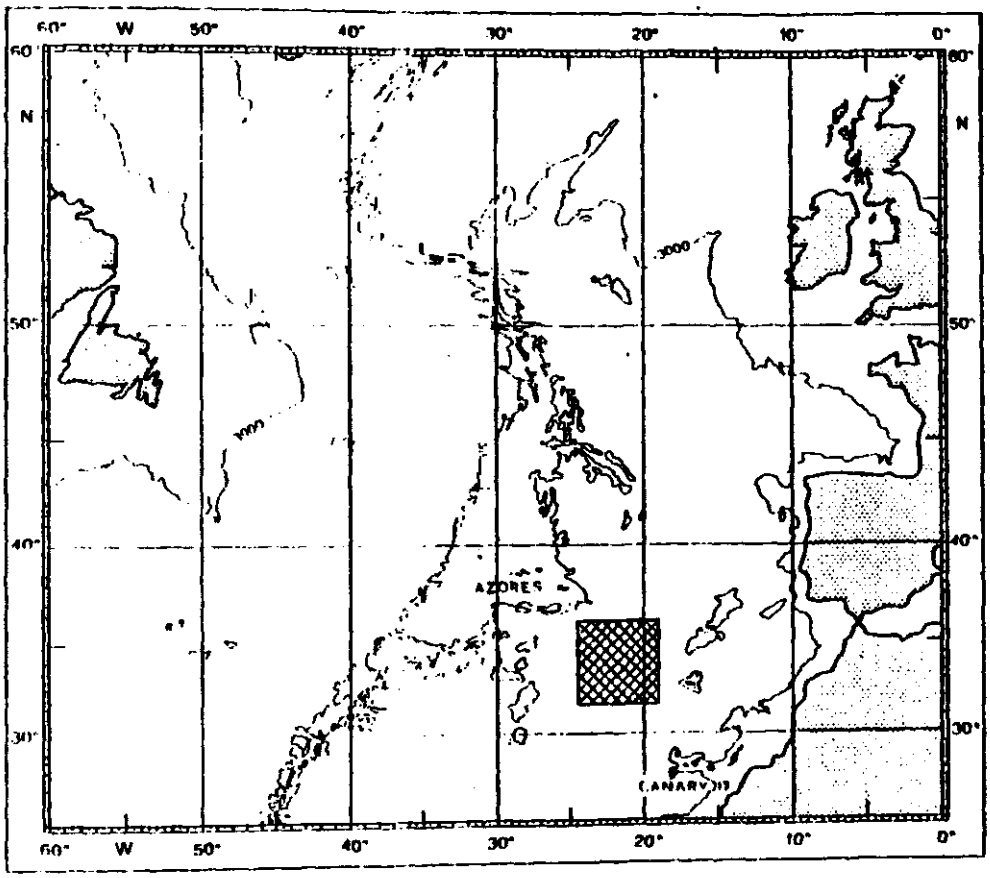

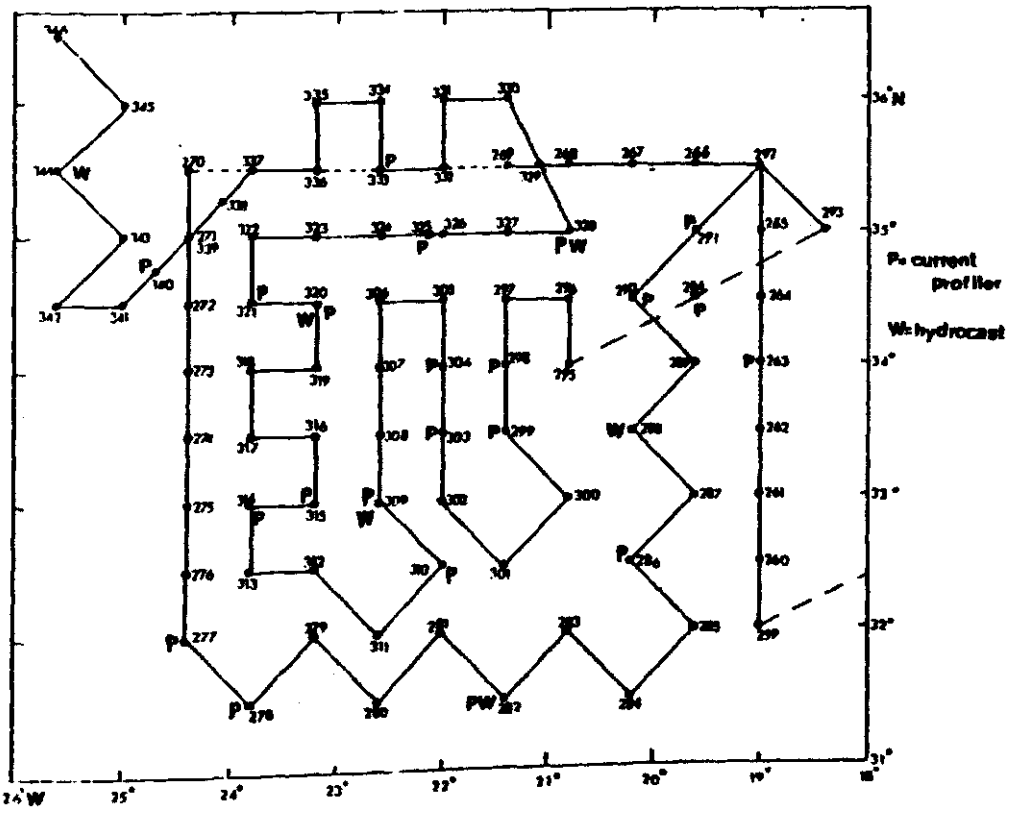

Fig. 1: a) Location of experiment POSEIDON 86 in spring 1982

b) Pattern of hydrographic survey

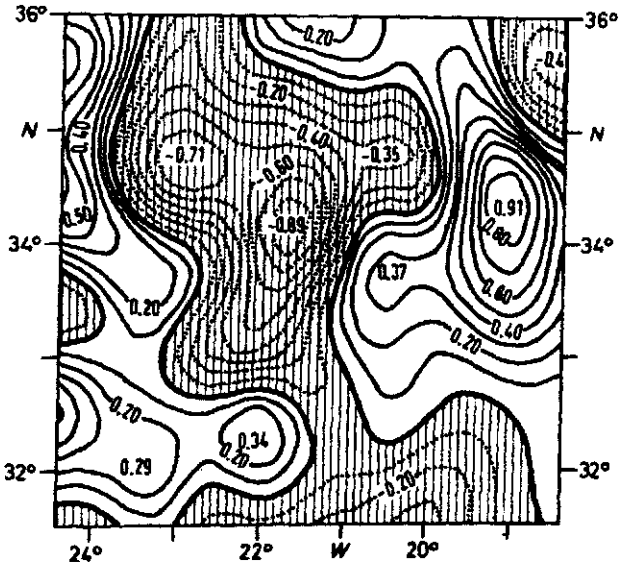

Fig. 2: a) Objective analysis of the geopotential anomaly field 25/1500 dBar ($m^2 s^{-2}$) with the approximate centre of the frontal band marked by the 13.5 $m^2 s^{-2}$ isoline

b) Objective analysis of the geopotential anomaly field 25/1500 dBar ($m^2 s^{-2}$) after subtraction of the linear spatial trend.

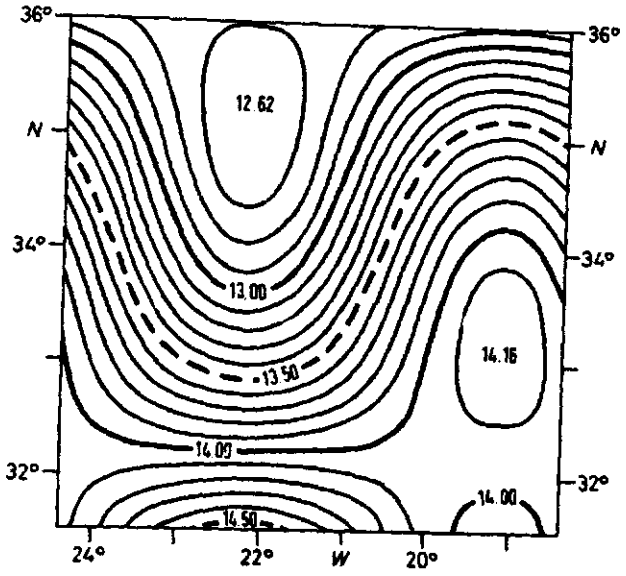

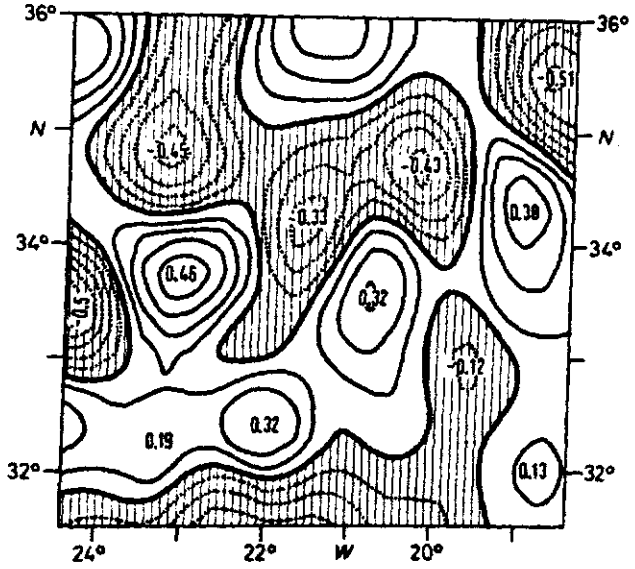

Fig. 2: c) Superposition of the linear spatial trend and the Rossby wave fit for the geopotential topography 25/1500 dBar ($m^2 s^{-2}$)
d) Objective analysis of the residual mesoscale perturbation field 25/1500 dBar ($m^2 s^{-2}$) after removal of the composite mean field.

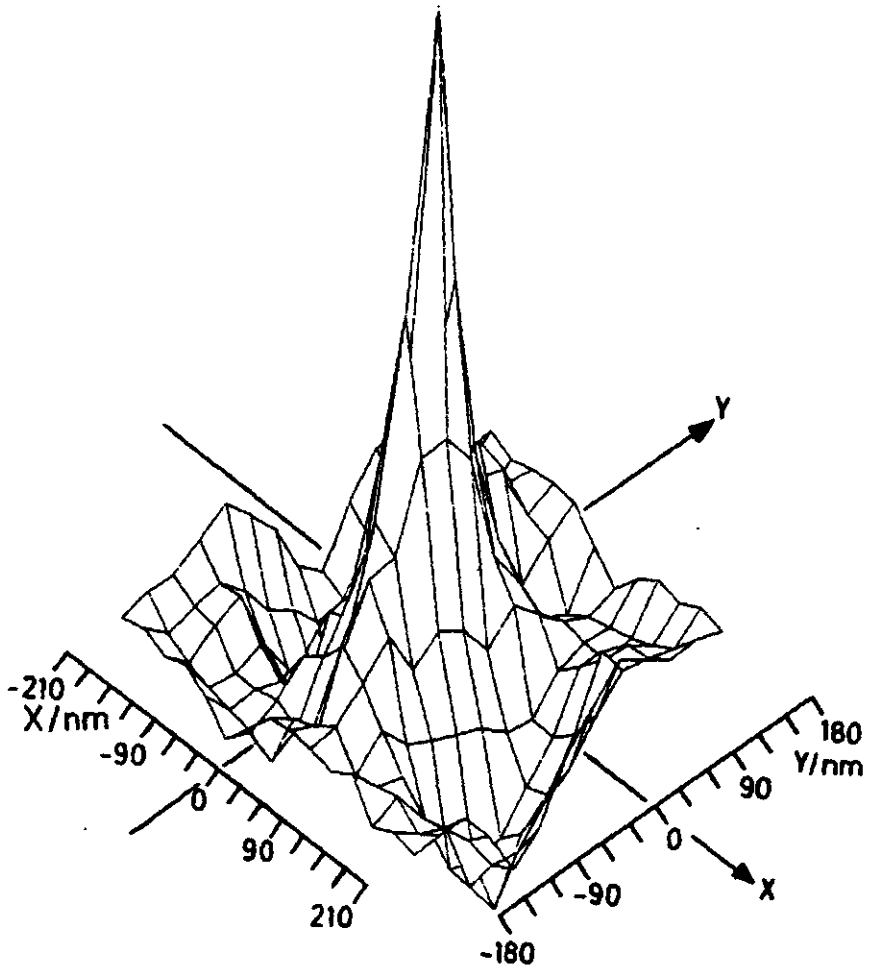

a)

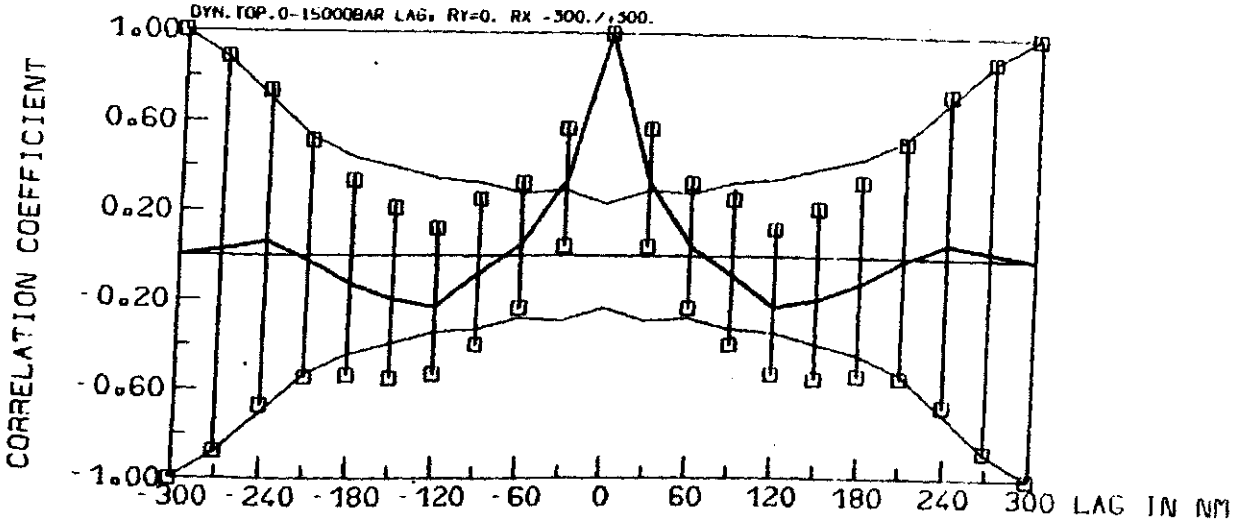

b)

Fig. 3: Two-dimensional raw correlations $\hat{C}(\underset{\sim}{r})$ of the geopotential anomaly field 25/1500 dBar shown with

a) lag vector $\underset{\sim}{r}$: $r_x \in (-210., 210.\ nm)$, $r_y \in (-180., 180.\ nm)$

b) [illegible] and corresponding error bars and

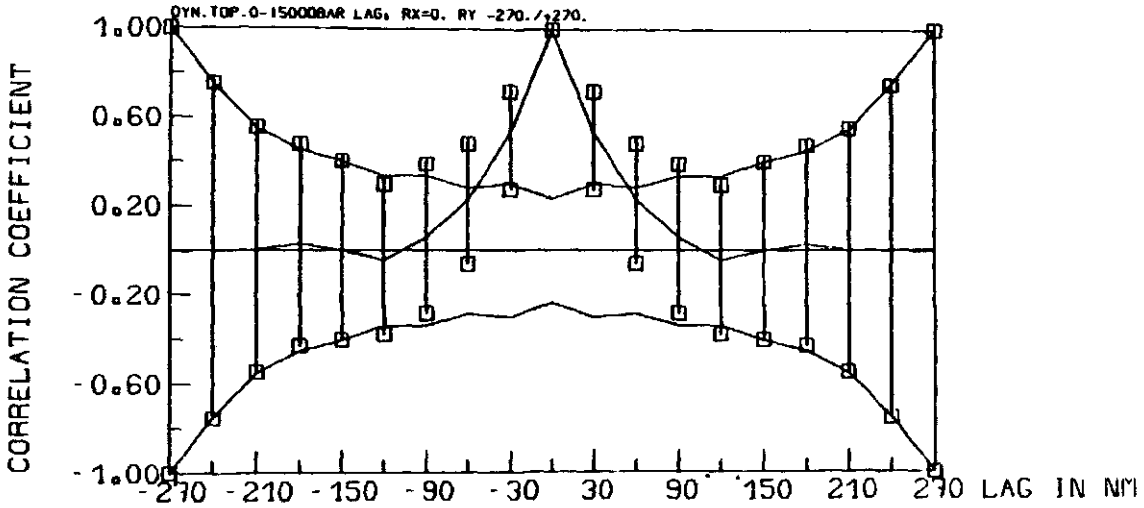

c)

Fig. 3: c)meridional separations and corresponding error bars and levels of zero-significance

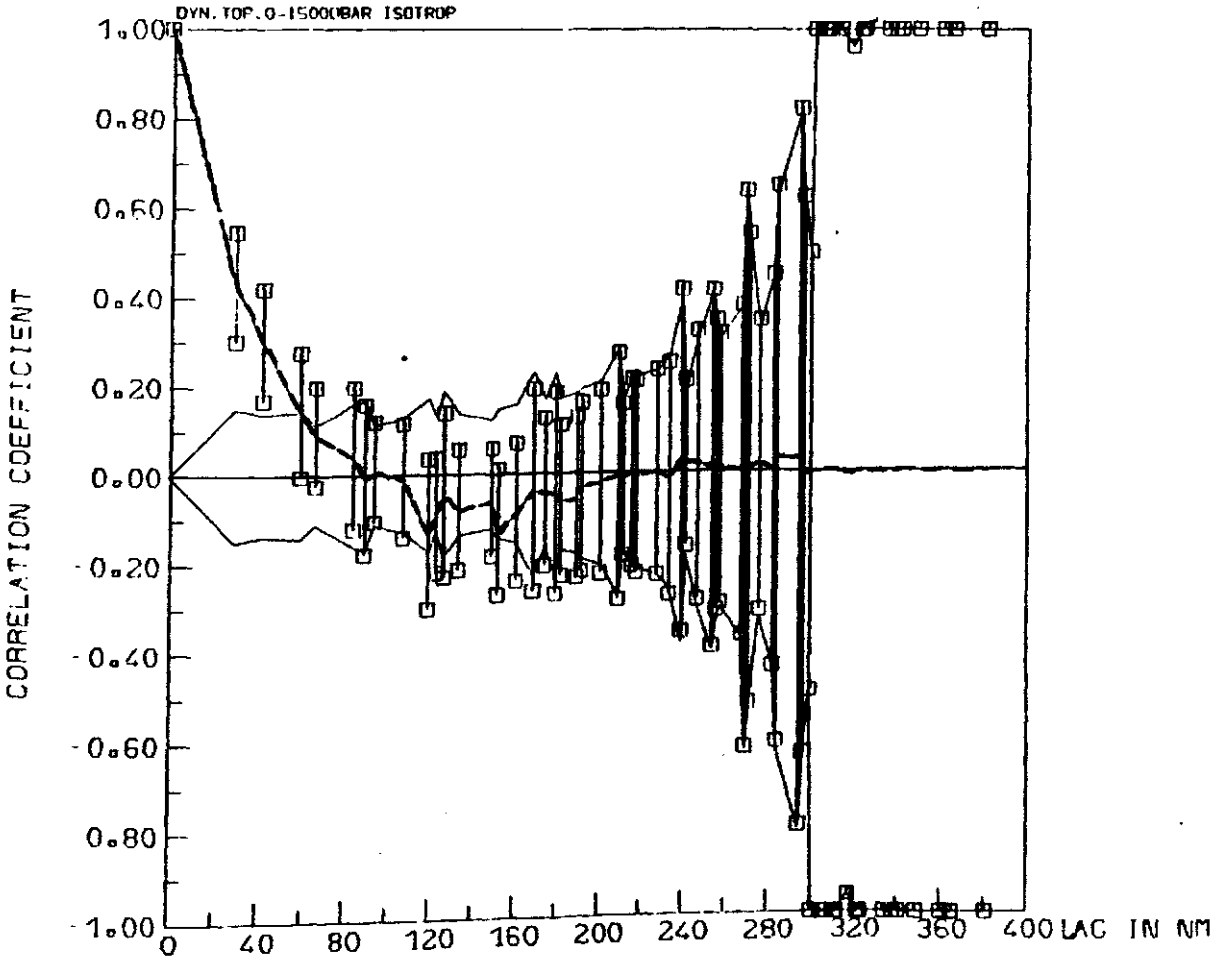

Fig. 4: Raw correlations of the geopotential anomaly field 25/1500 dBar computed with the assumption of isotropy with error bars and levels of zero-significance.

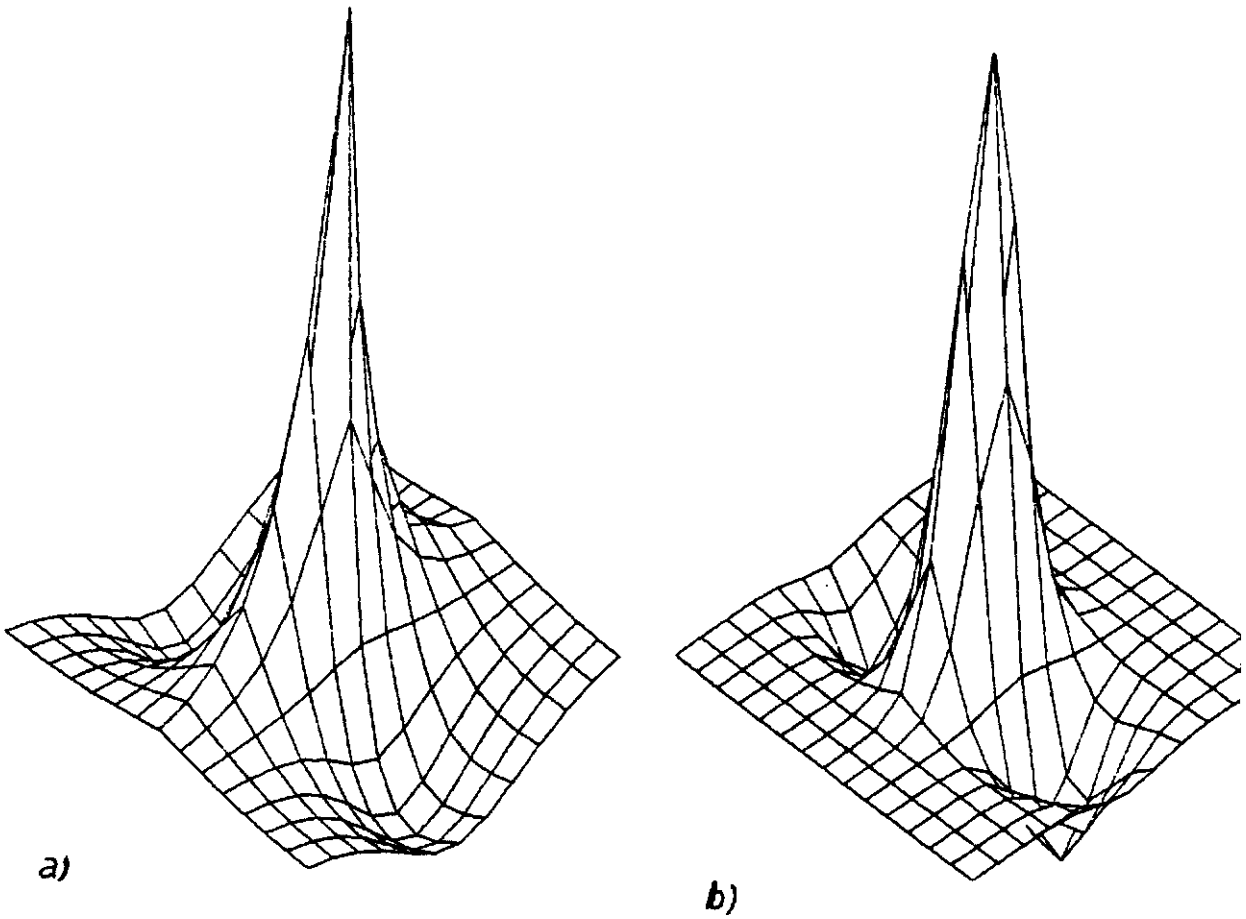

Fig. 5: Plots of the fitted model correlation functions

a) case 2 of table 1
b) case 3 of table 1

(Results of model classes case 1, 4, are not shown being equivalent to case 7 (see table 1))

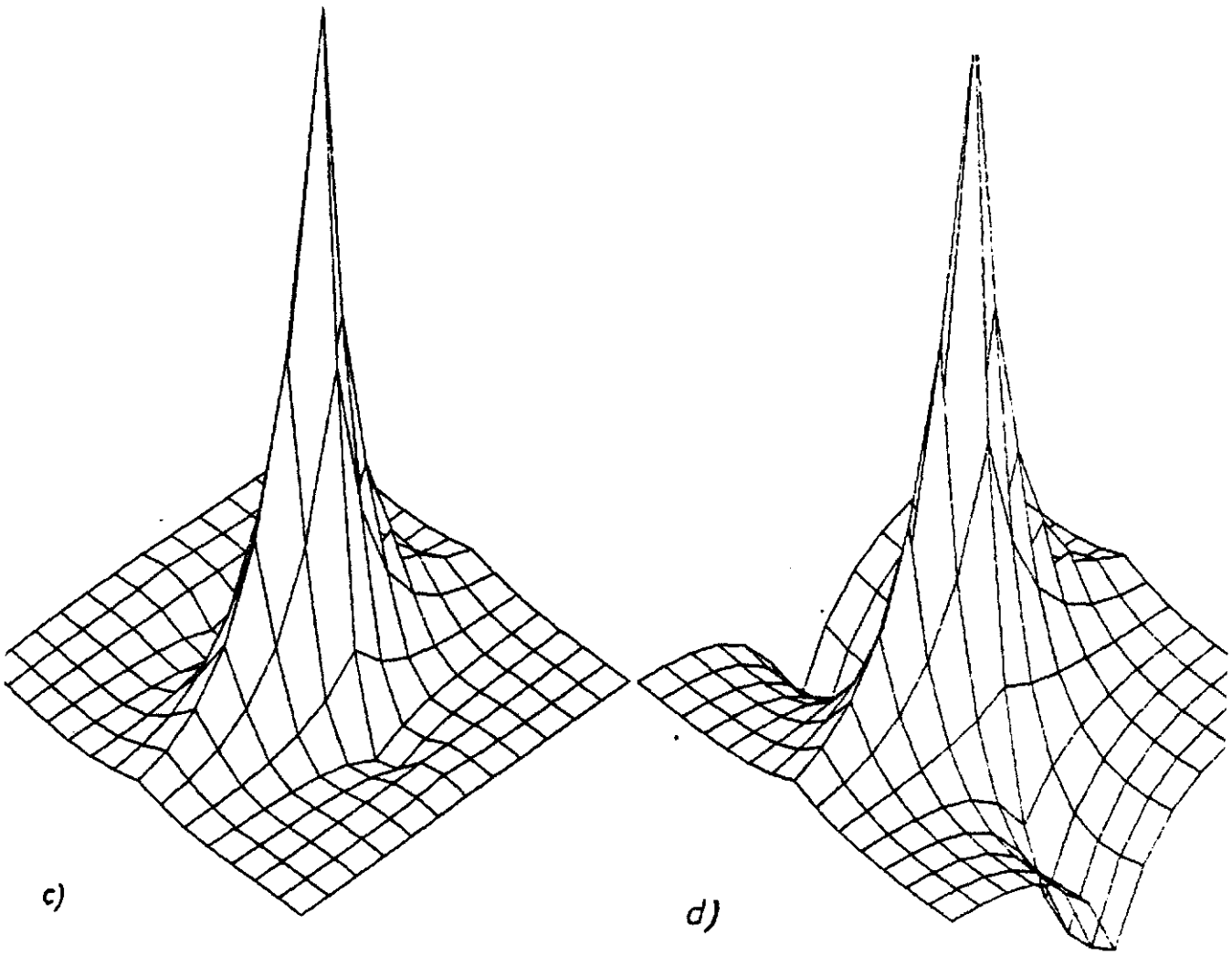

Fig. 5: Plots of the fitted model correlation functions

c) case 5 of table 1
d) case 6 of table 1

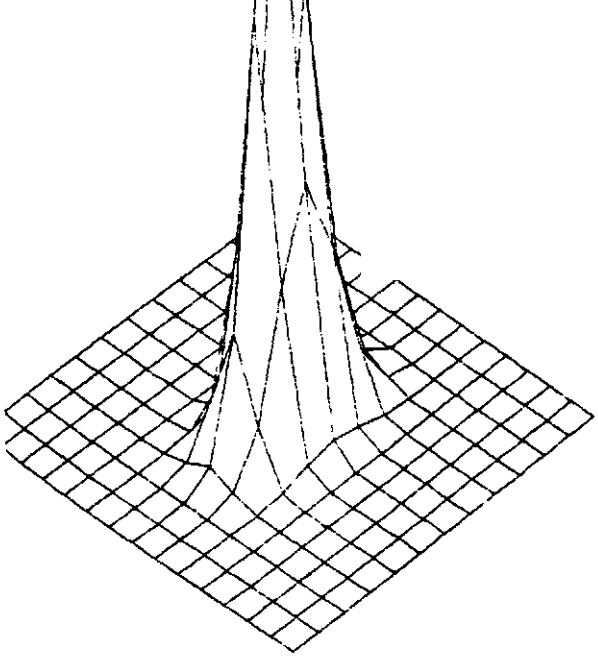

e)

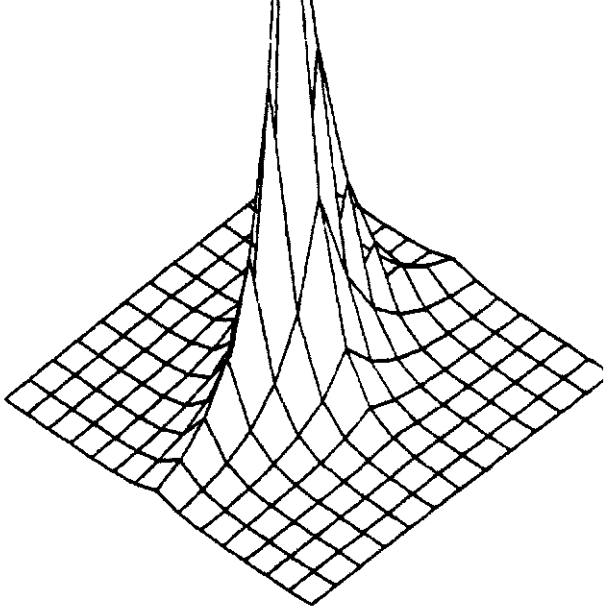

f)

Fig. 5: Plots of the fitted model correlation functions

e) case 7 of table 1
f) case 8 of table 1

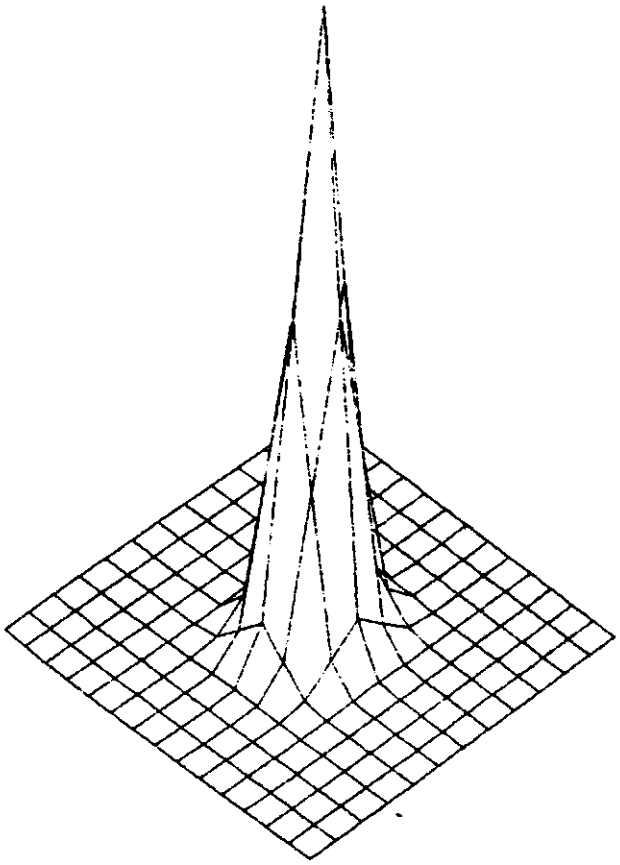

g)

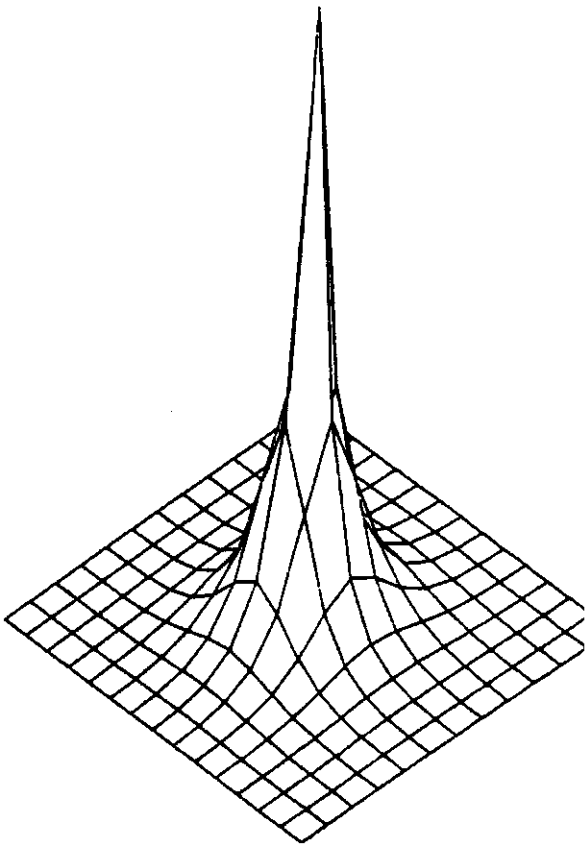

h)

Fig. 5: Plots of the fitted model correlation functions

g) case 9 of table 1
h) case 10 of table 1

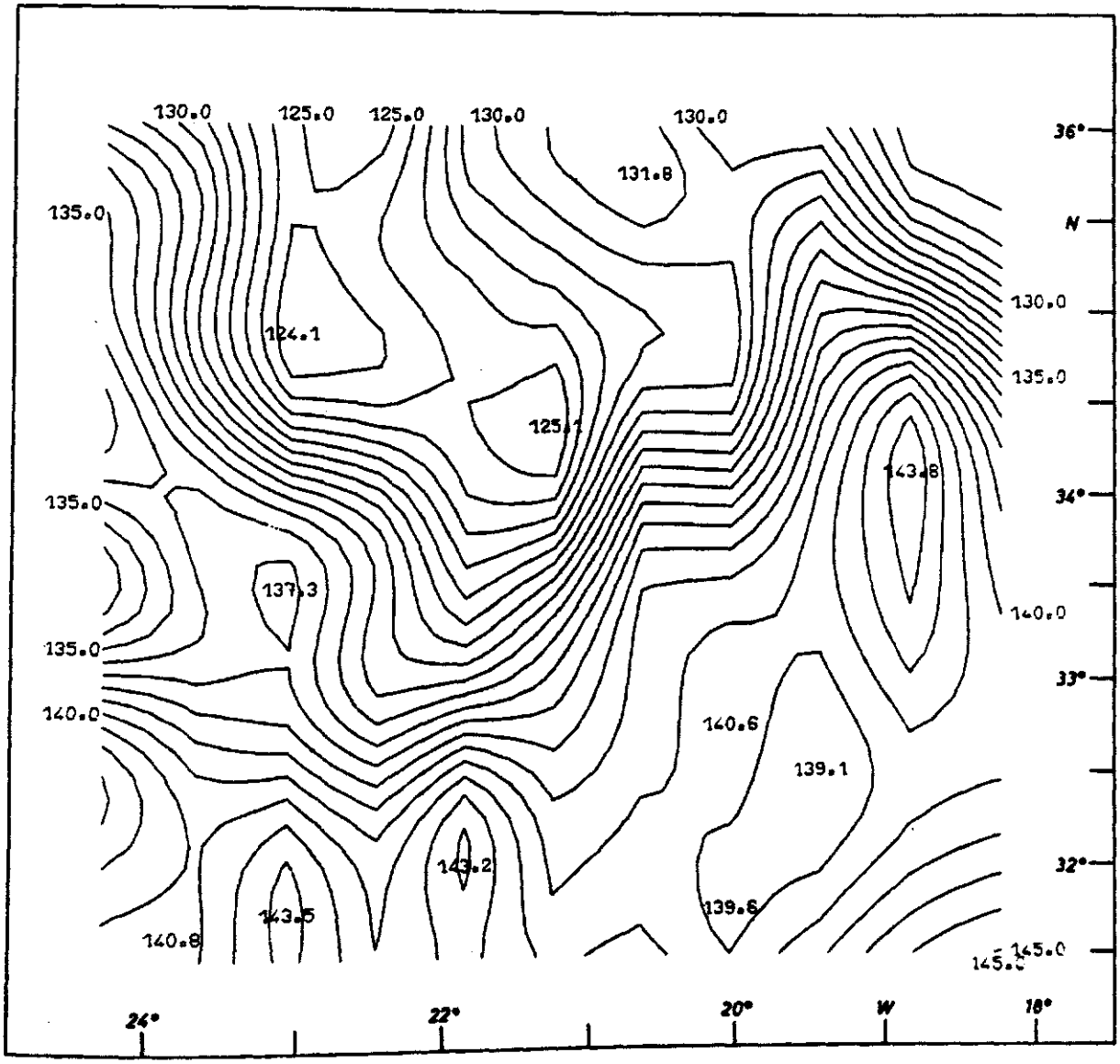

Fig. 6: Maps of geopotential anomaly 25/1500 dBar ($10^{-1}m^2s^{-2}$) computed with different covariance functions

a) case 3 of table 1

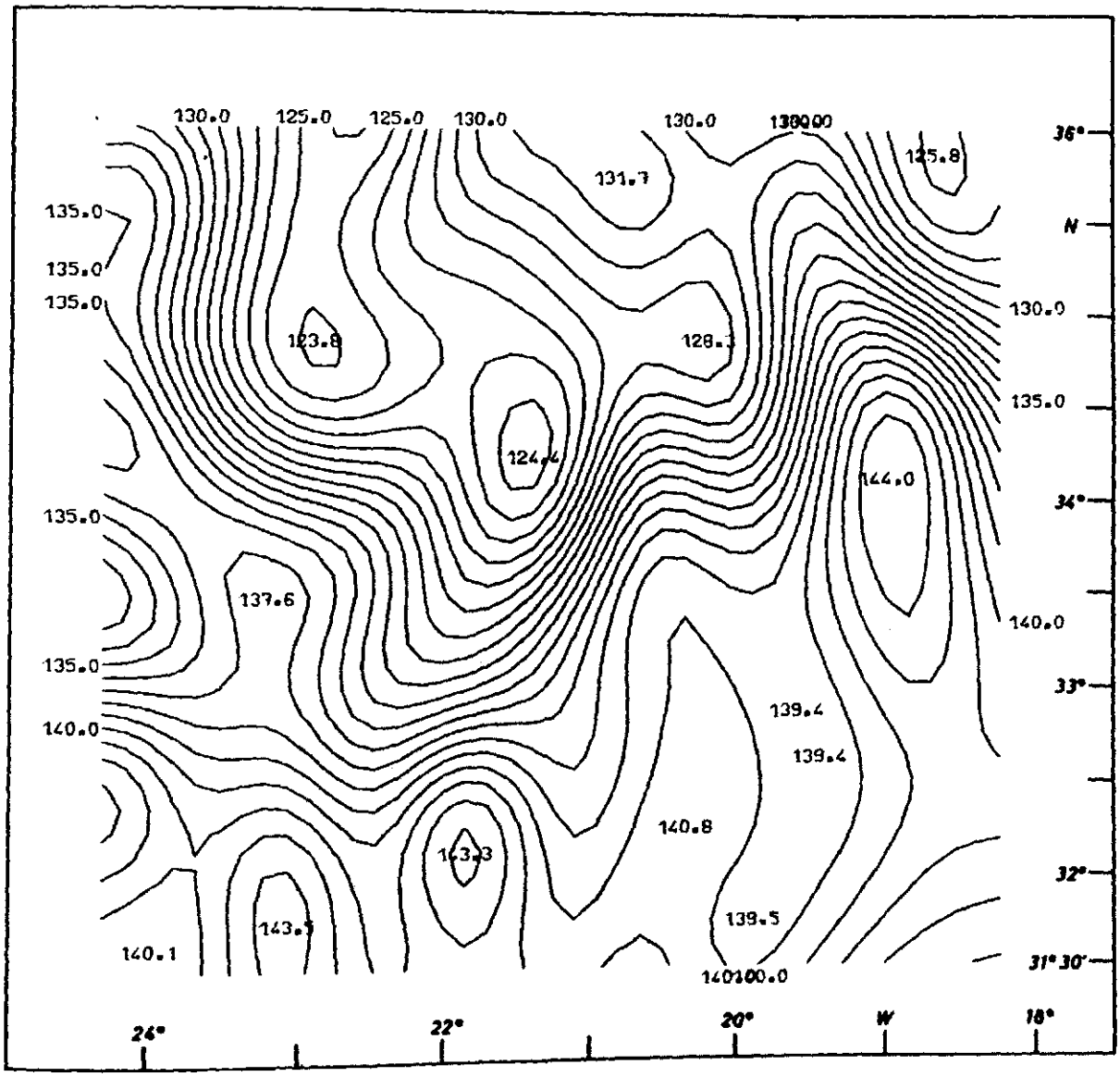

Fig. 6: Maps of geopotential anomaly 25/1500 dBar ($10^{-1}m^2s^{-2}$) computed with different covariance functions

b) case 7 of table 1

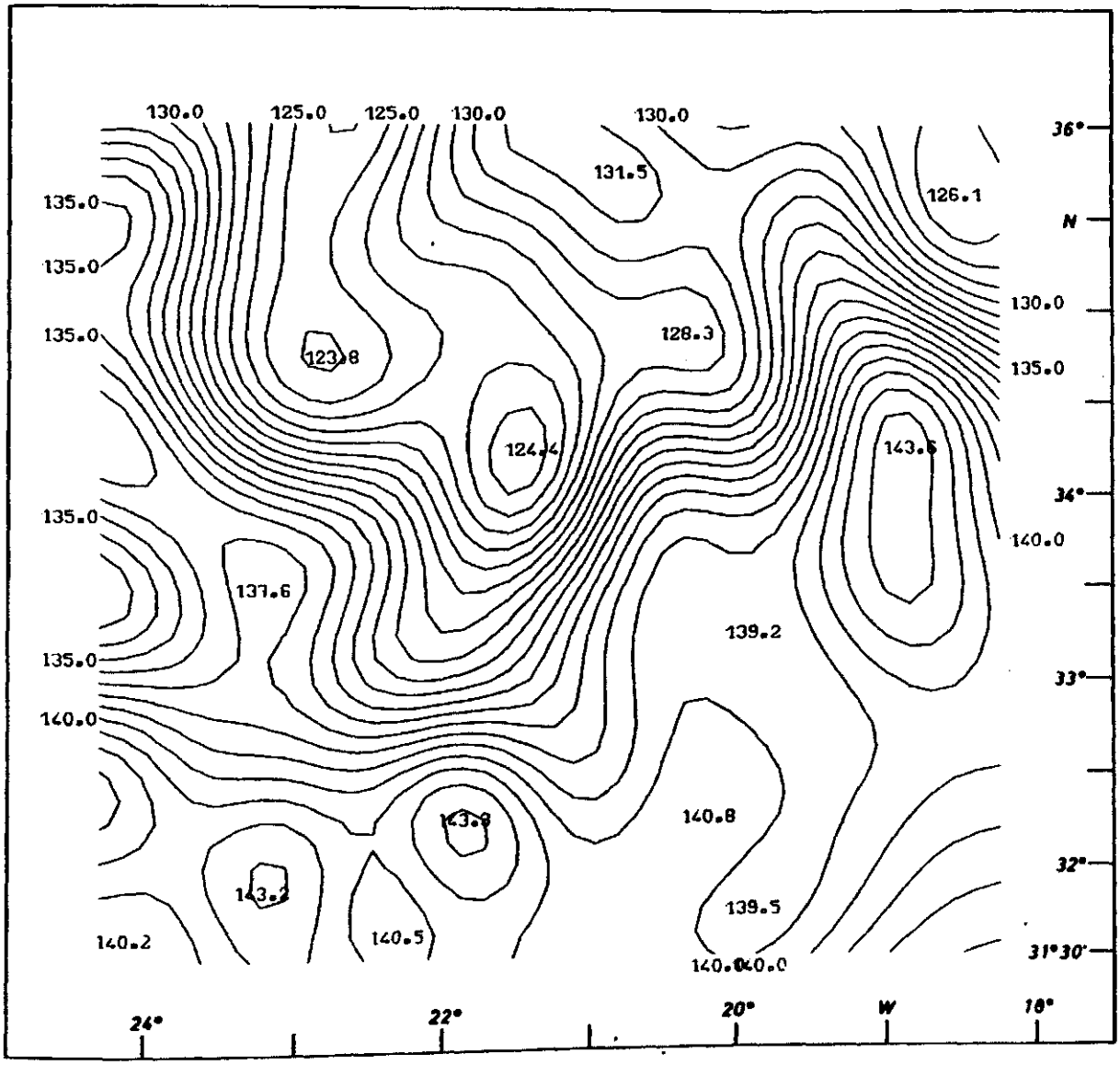

Fig. 6: Maps of geopotential anomaly 25/1500 dBar ($10^{-1}m^2s^{-2}$) computed with different covariance functions

c) case 9 of table 1

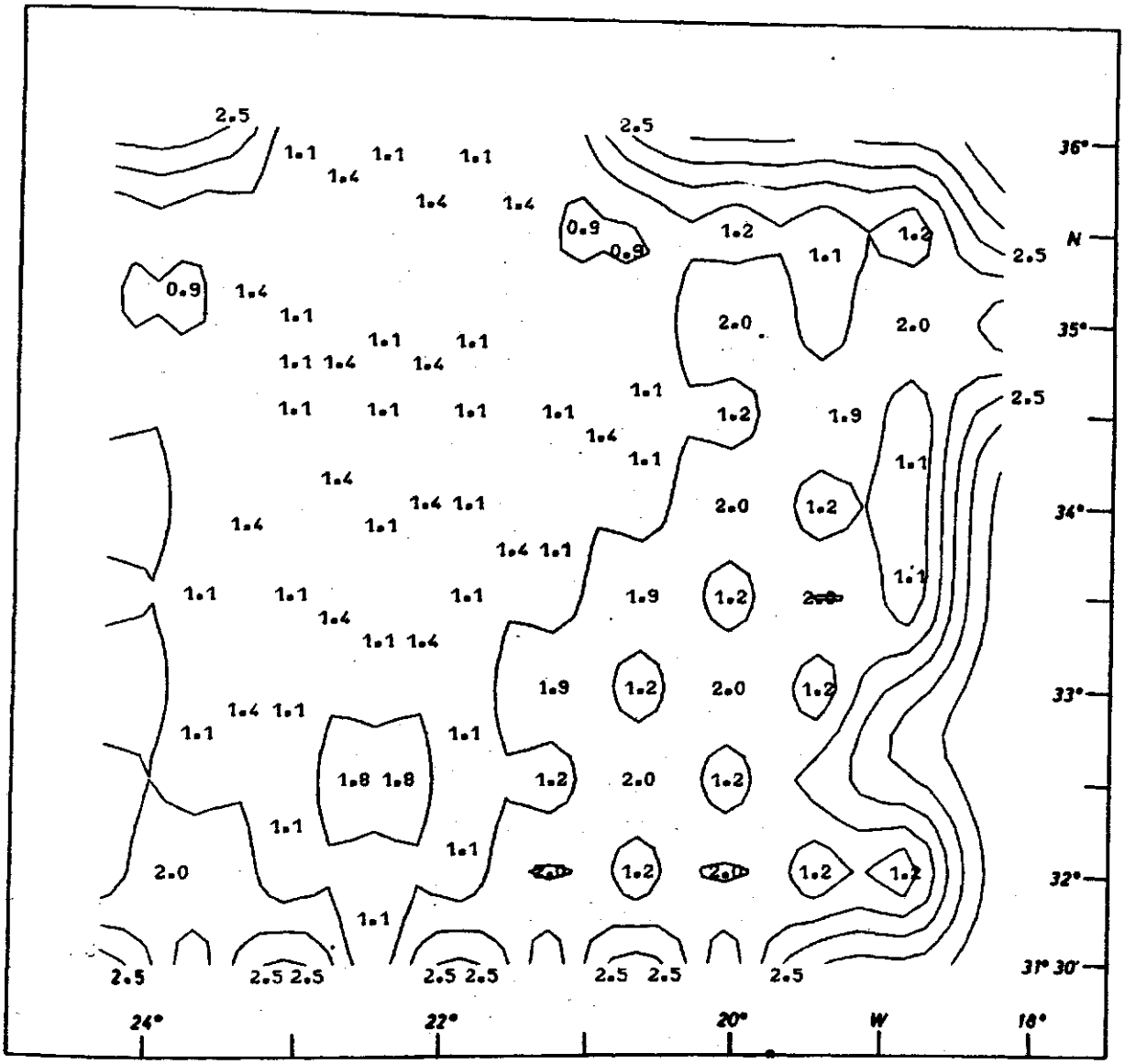

Fig. 7: a) rms error field - contoured every .5 ($10^{-1}m^2s^{-2}$)

7a)

b) anomaly field (dyn cm) of the geopotential anomaly map 25/1500 dBar computed with the covariance function (case 7, table 1) chosen for the final analysis

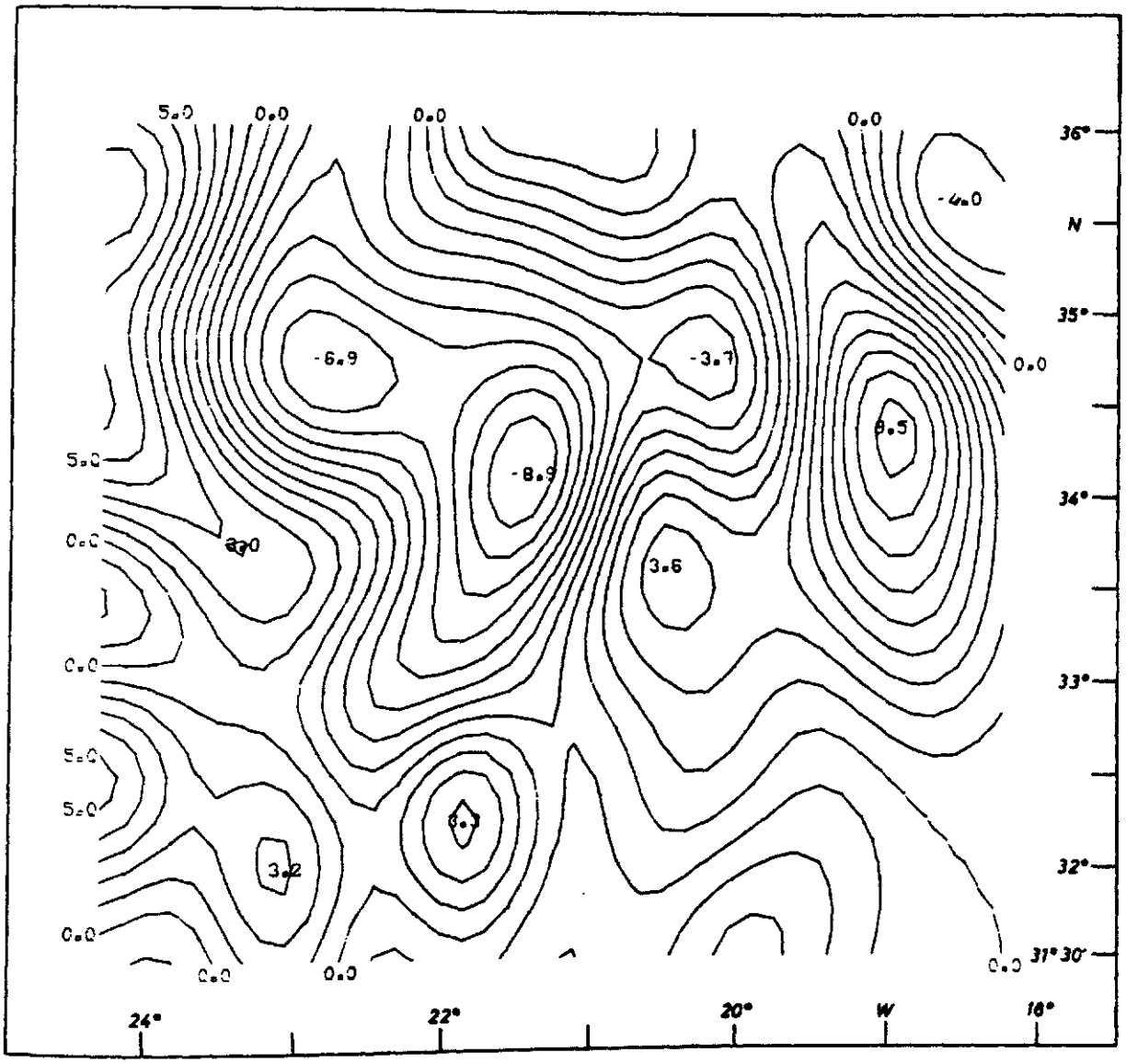

Fig. 7: b) anomaly field ($10^{-1}m^2s^{-2}$) of the geopotential anomaly map 25/1500 dBar with the covariance function (case 7, table 1) chosen for the final analysis

7b)

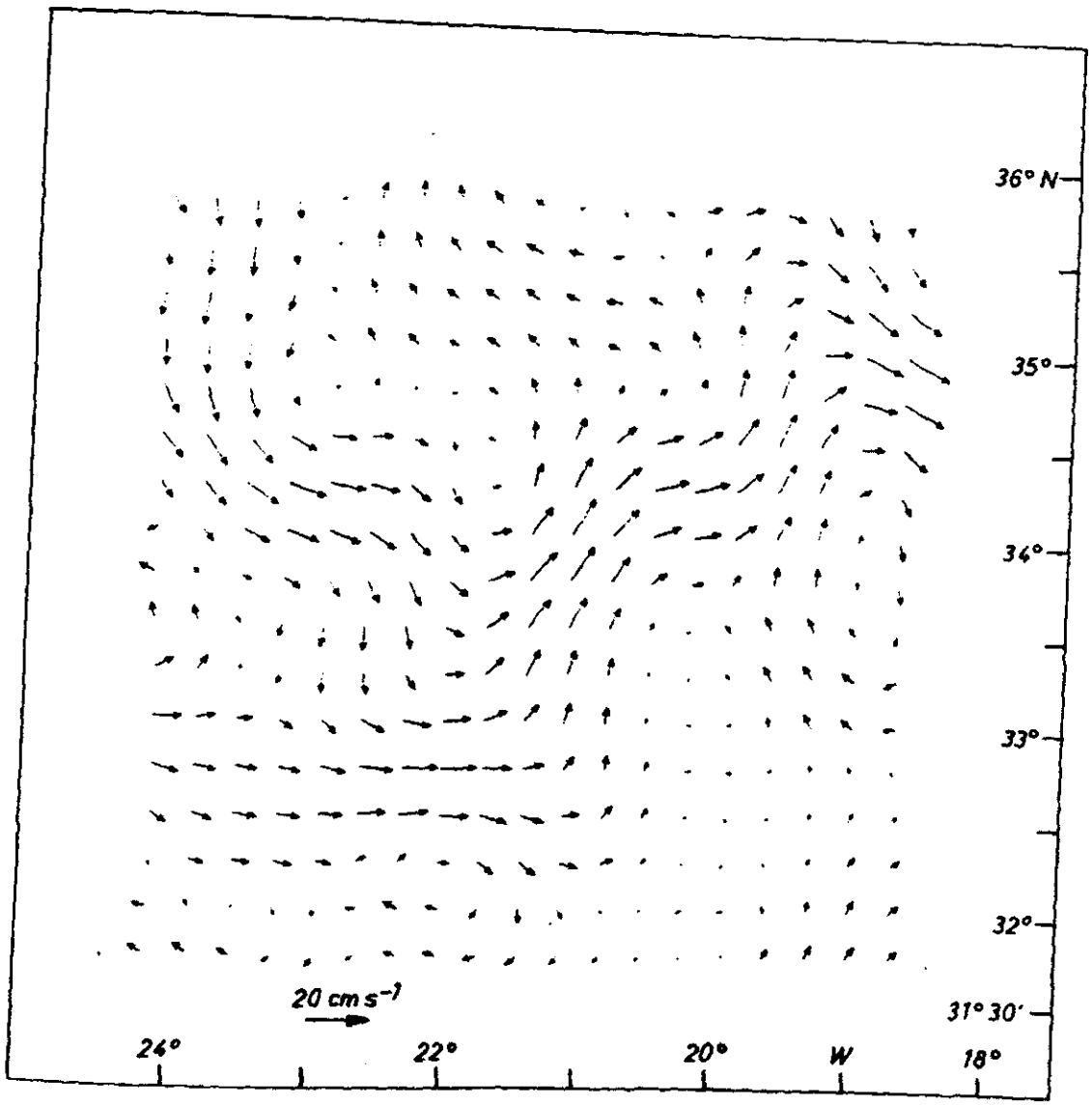

8.a)

Fig. 8: Geostrophic velocity field

a) for the total geopotential anomaly field 25/1500 dBar computed with the covariance function (case 7, table 1) chosen for the final analysis

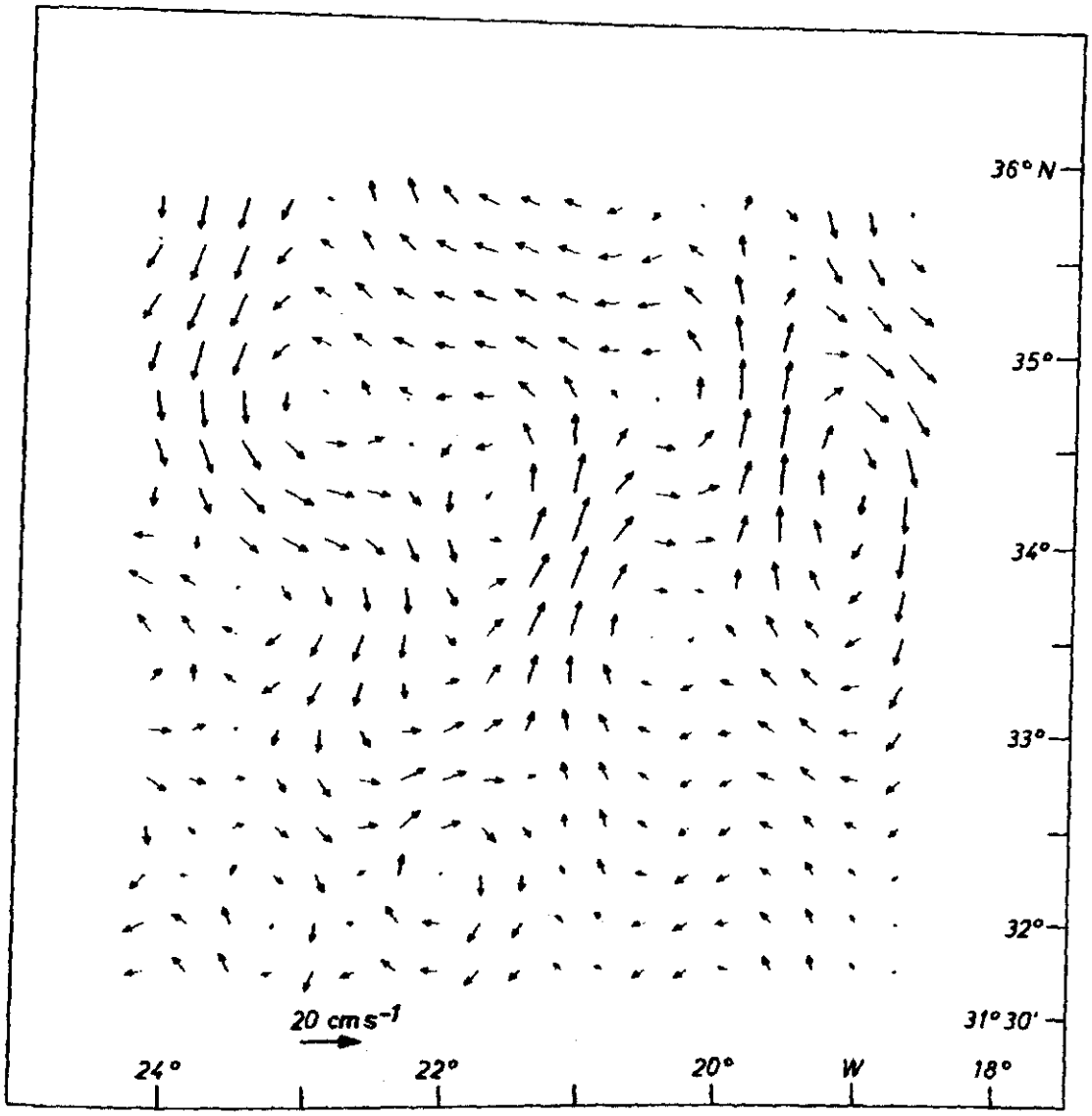

8.b)

Fig. 8: Geostrophic velocity field

a) for the total geopotential anomaly field 25/1500 dBar computed with the covariance function (case 7, table 1) chosen for the final analysis

b) for the anomaly geopotential topography field 25/1500 dBar respectively

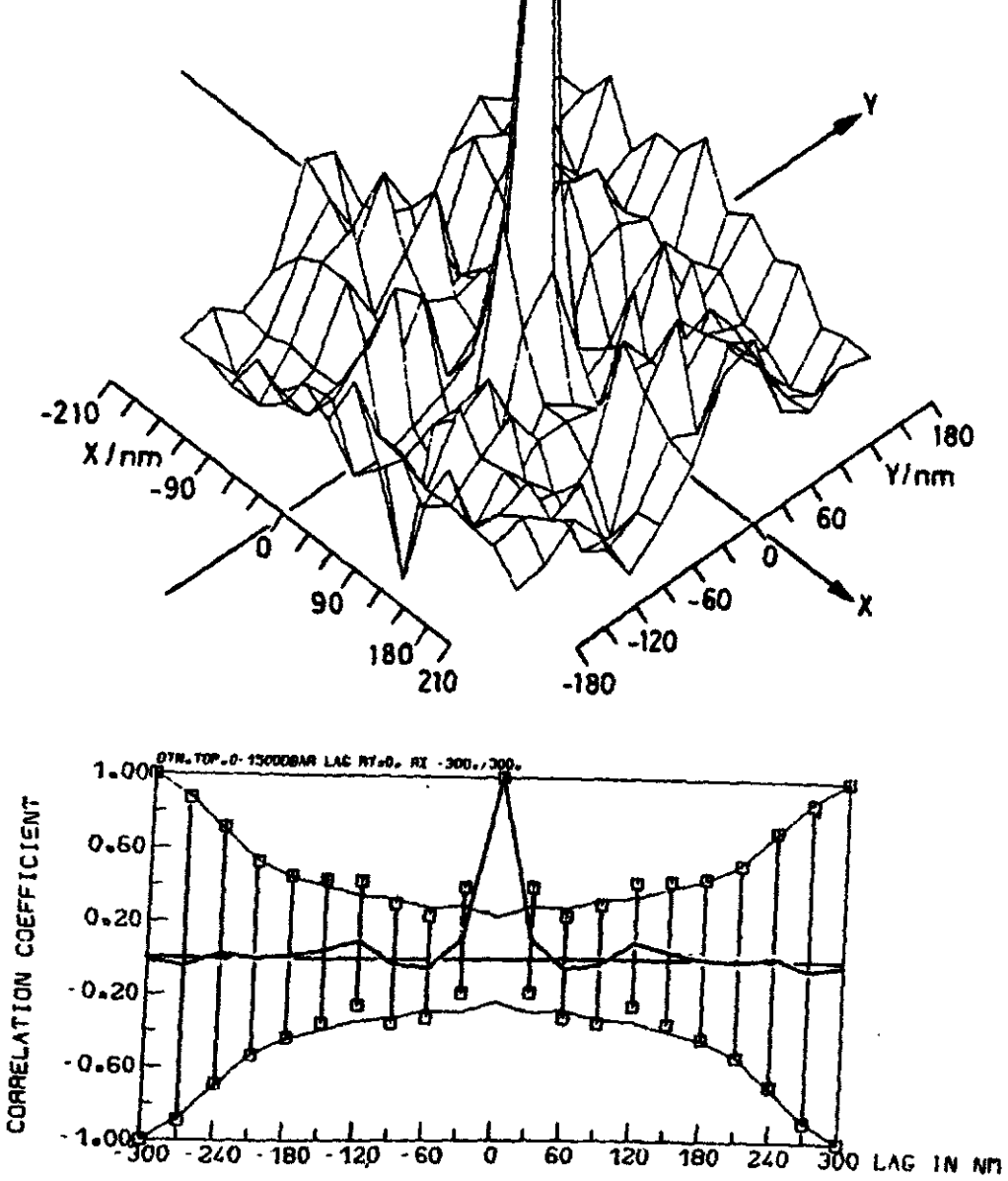

Fig. 9: Two-dimensional raw correlations $\hat{C}(\underset{\sim}{r})$ of the mesoscale perturbations in the geopotential anomaly field 25/1500 dBar shown with

a) lag vector $\underset{\sim}{r}$: $r_x \varepsilon(-210.,210.$ nm),
$r_y \varepsilon(-180.,180.$ nm)

b) Zonal separations: $r_x \varepsilon(-300.,300.$ nm)
$r_y = 0$

and corresponding error bars and levels of zero significance

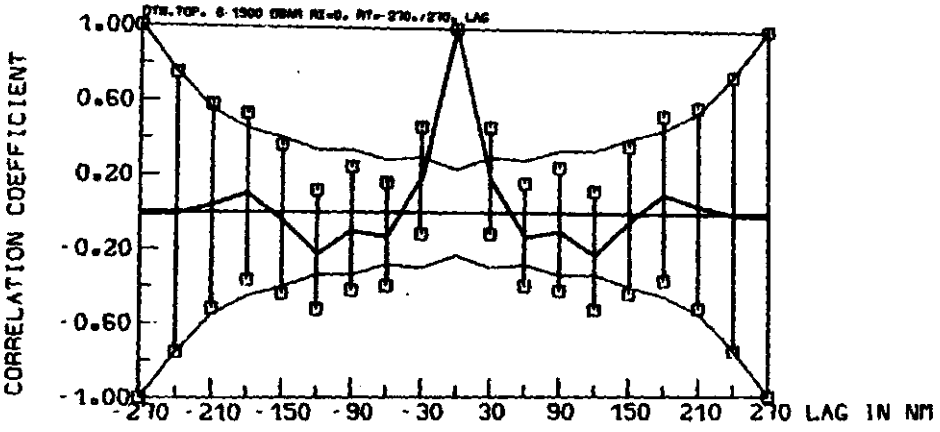

Fig. 9: c) meridional separations $r_x=0$
$r_y \varepsilon(-270.,270.\ nm)$
and corresponding error bars and levels of zero significance.

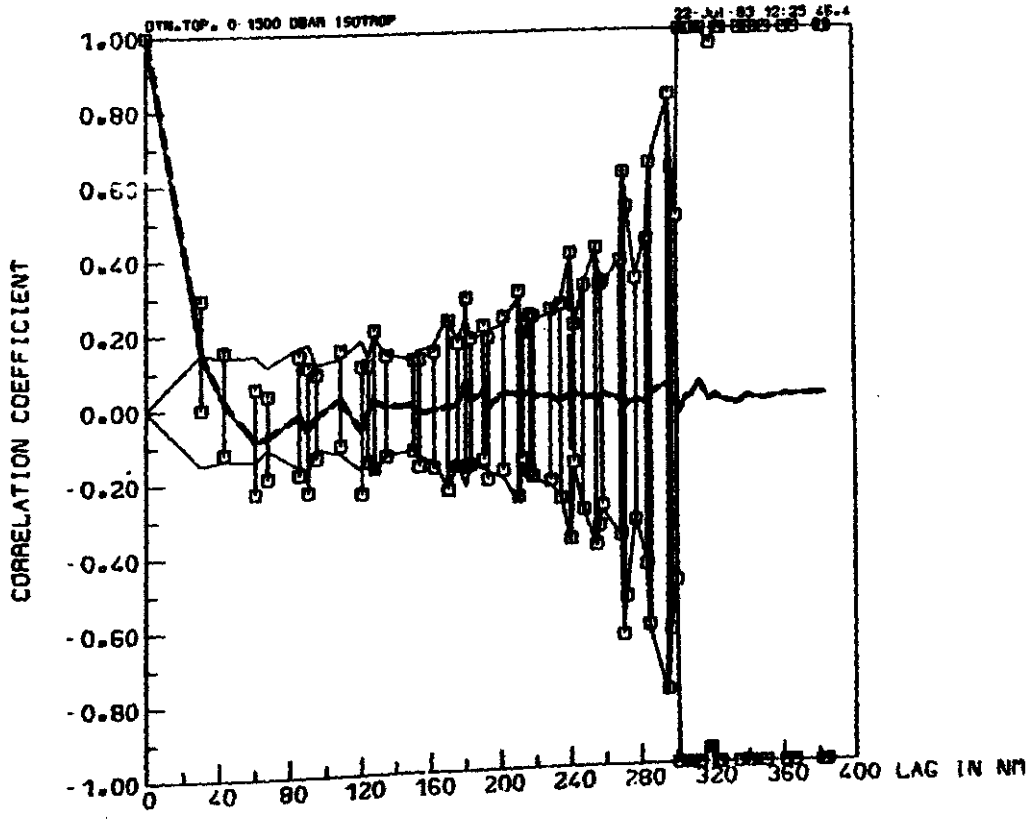

Fig. 10: Raw correlations $\hat{C}(|\underline{r}|)$ of the mesoscale perturbations in the geopotential anomaly field 25/1500 dBar computed with the assumption of isotropy with error bars and levels of zero significance.

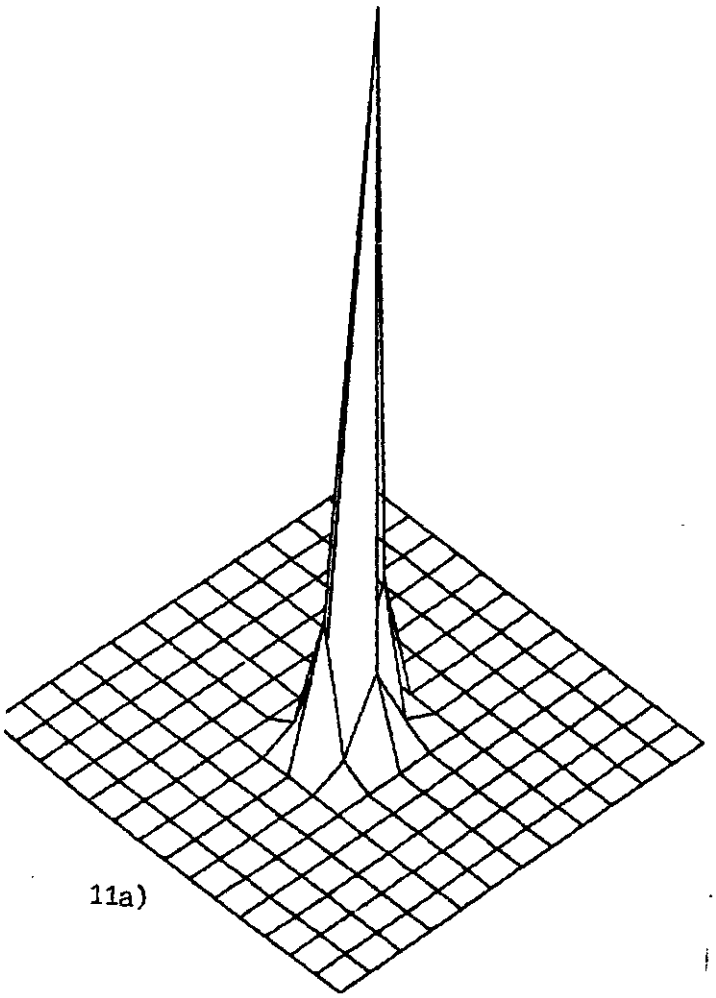

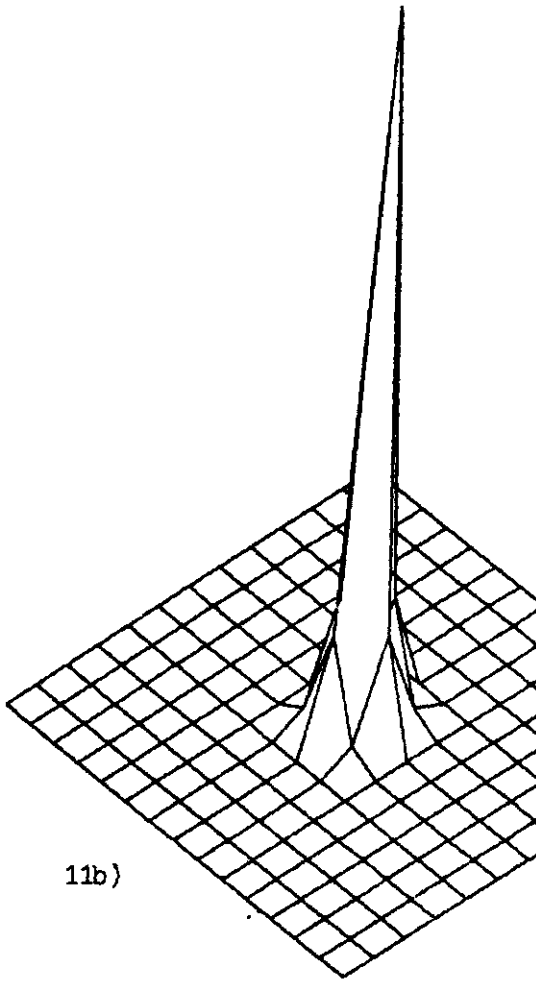

Fig. 11: Plots of the fitted model correlation functions
a) case 1 of table 2
b) case 2 of table 2

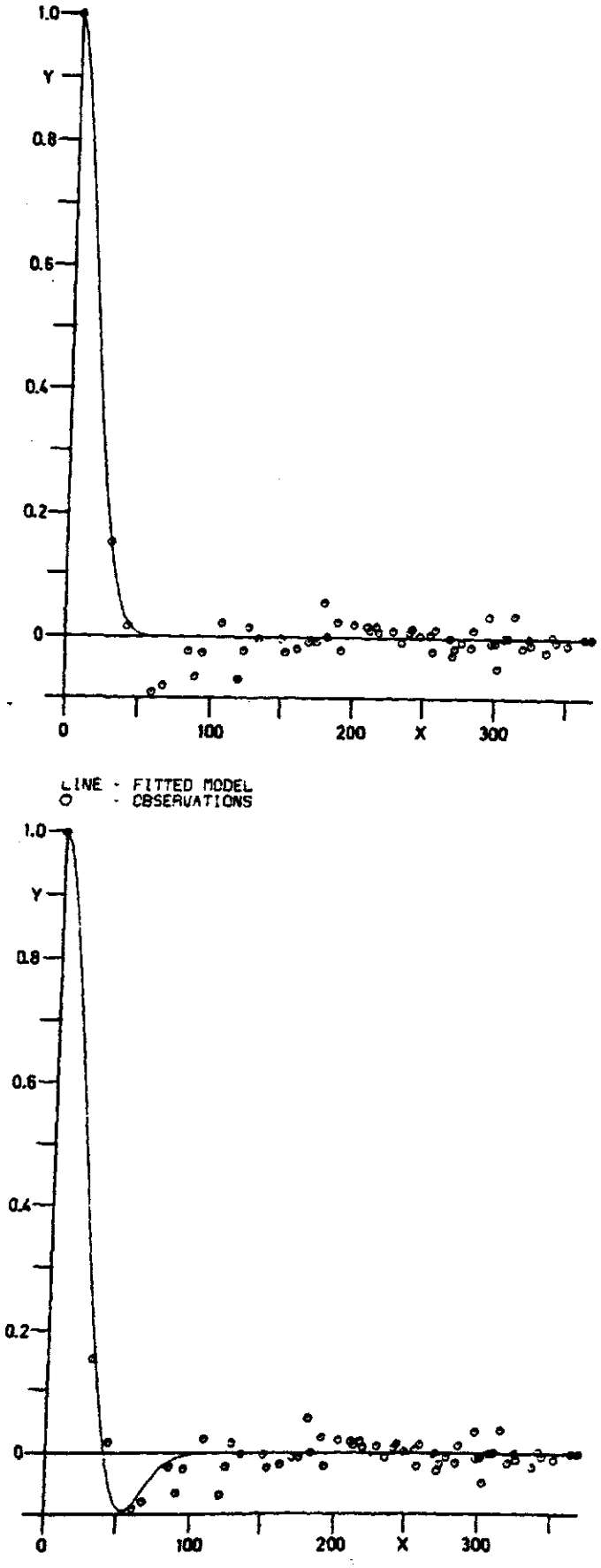

Fig. 12: Plots of the fitted isotropic model correlation functions
a) case 3 of table 2
b) case 4 of table 2

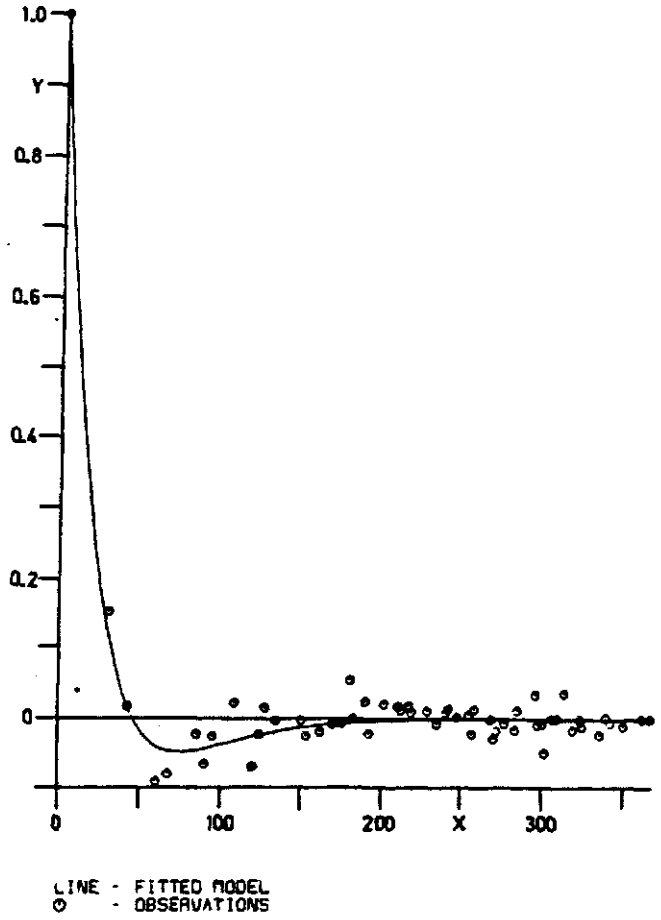

Fig. 12: Plots of the fitted isotropic model correlation functions
c) case 5 of table 2

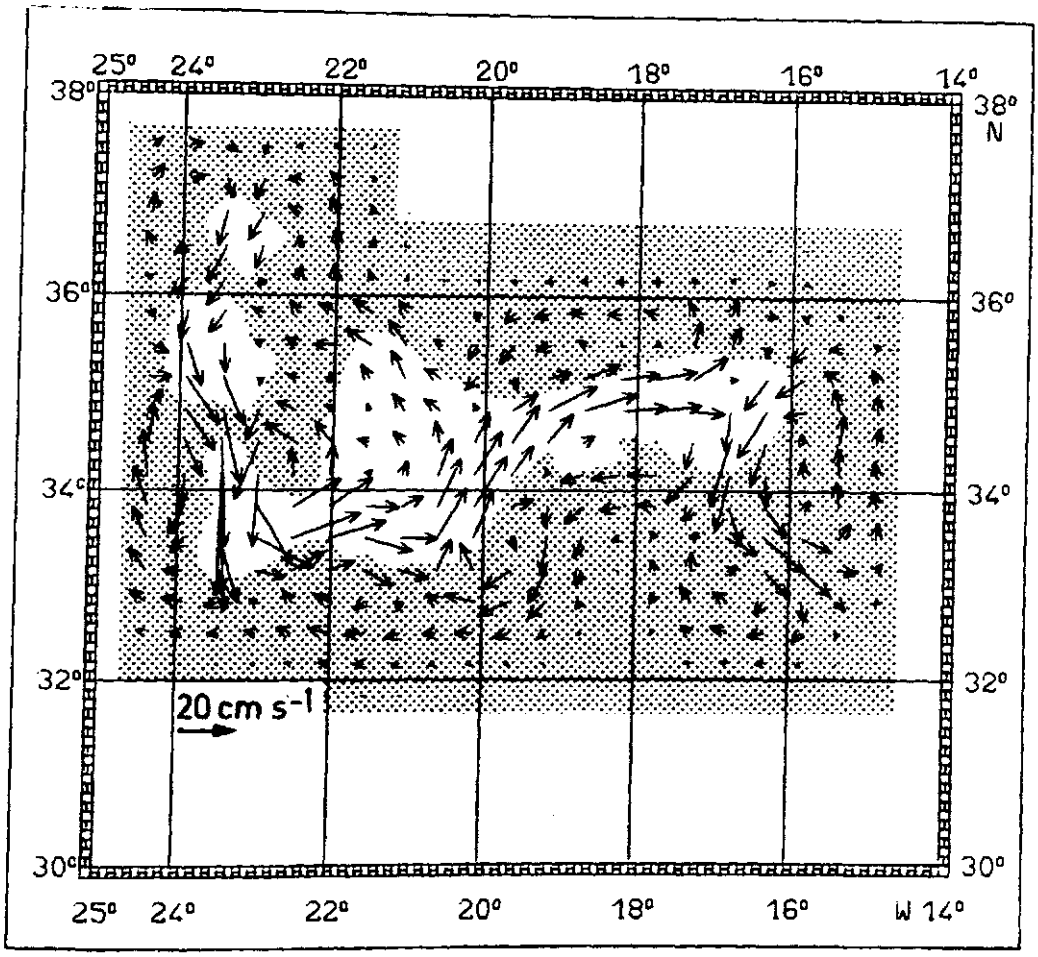

Fig. 13a): Objective Analysis of a quasi-Eulerian velocity field as derived from driftbuoy trajectories. The correlation scale is λ = 75 km and the error variance is assumed to be 10 % of the total variance.
In the dotted area the error variance exceeds 50 % of the total variance. Due to the sparsity of data and the choice. of the correlation scale, the region of reliable velocity estimates is small and patchy.

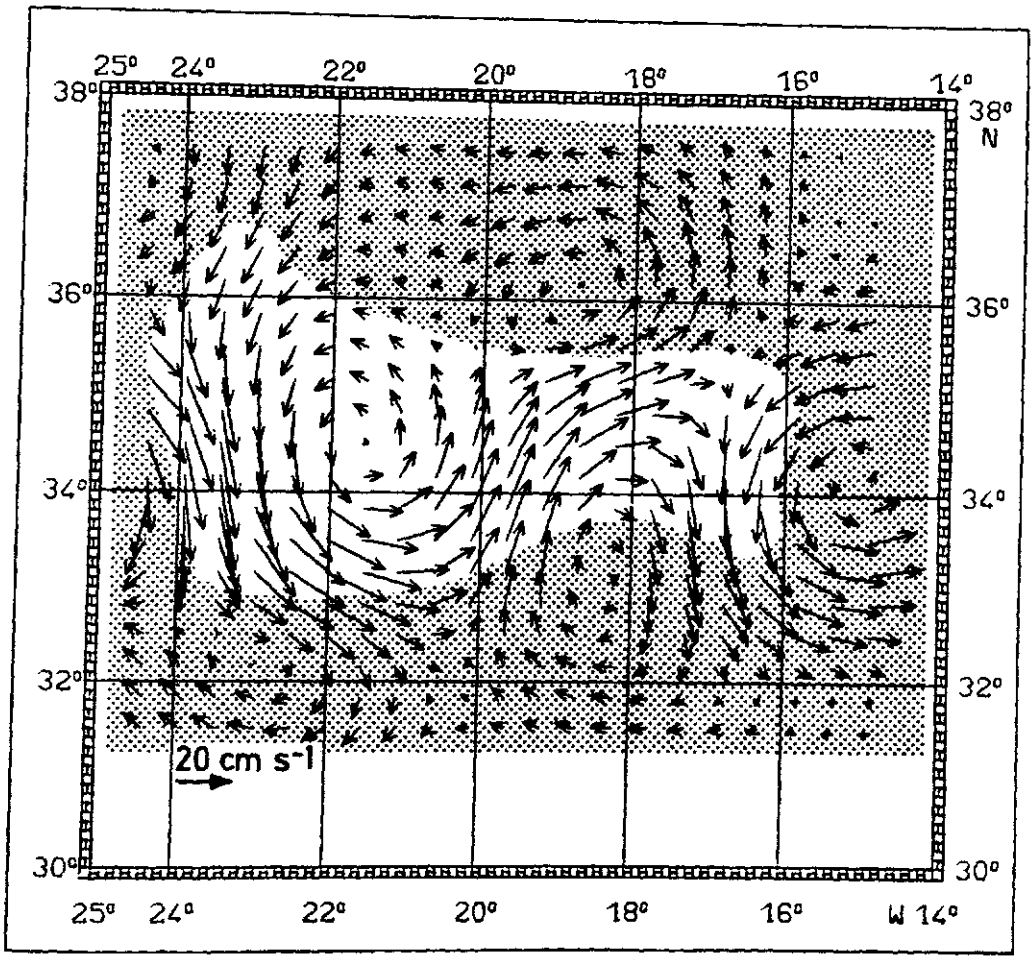

Fig. 13b): Objective Analysis of the same input velocity field as in Fig. 13a) with correlation scale λ = 200 km and assumed noise variance 30 % of the total variance of the field. By this approach mesoscale variability on scales smaller than 200 km is treated as noise and essentially smoothed out. In the dotted area the error variance exceeds 50 % of the total variance.

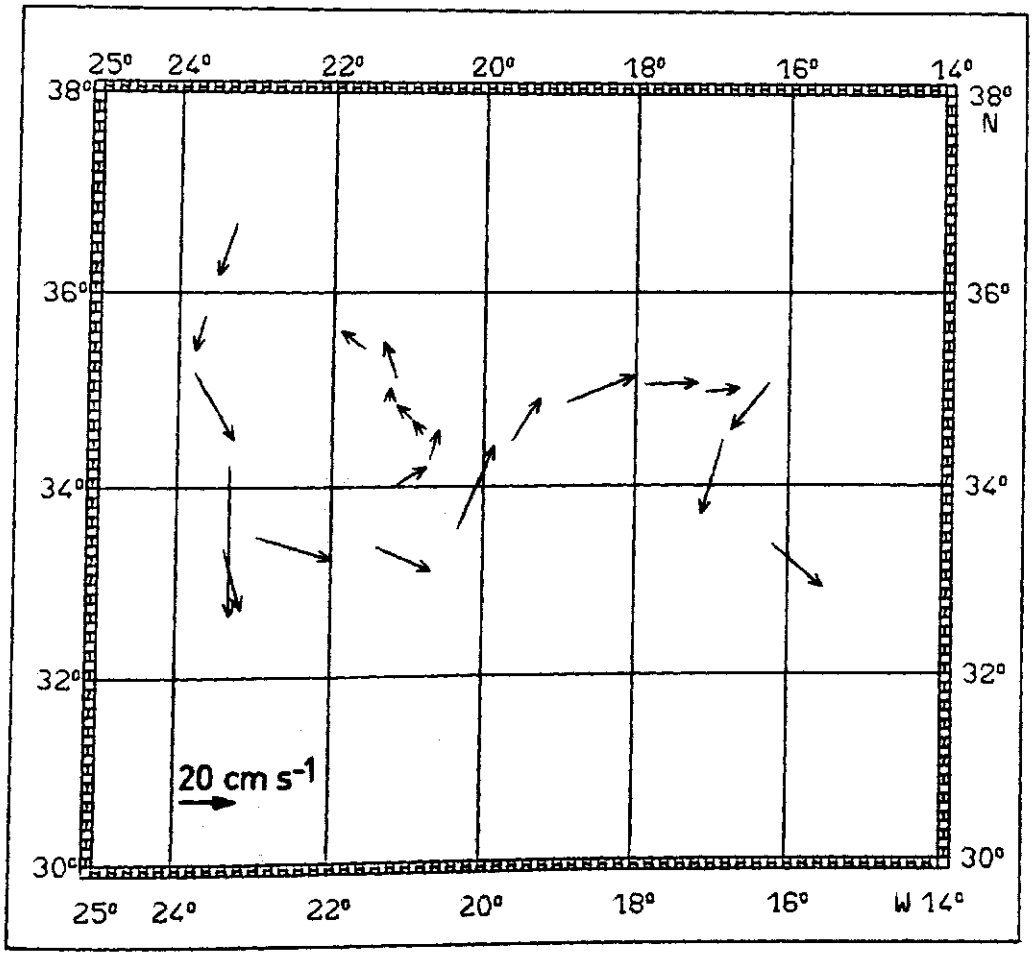

Fib. 13c): Input velocity field for the estimated velocity fields shown in Fig. 13a) and 13b)

SOURCE OF VARIATION	DEGREES OF FREEDOM	SUMS OF SQUARES	MEAN SQUARES
REGRESSION	2.00000	1487.67900	743.83950
RESIDUAL	70.00000	1164.84360	16.64062
TOTAL	72.00000	2652.52260	

F-VALUE FOR NULL HYPOTHESIS TEST
(ALL REGRESSION PARAMETER ZERO)

44.70022

PROBABILITY OF EXCEEDING F UNDER ASSUMPTION OF THE NULL HYPOTHESIS

0.00000

PERCENTAGE OF VARIATION EXPLAINED	STAND. DEVIATION OF RESIDUALS	STD. DEV. AS PERCENTAGE OF RESPONSE MEAN
56.08544	4.07929	3.04220

REGRESSION COEFFICIENT INTERFERENCES

DIGITS OF ACCURACY FOR REGRESSION COEFF. ESTIMATES

4.0

VARIABLE NUMBER I	MEAN	REGRESSION COEFFICIENT	LOWER CONFID. LIMIT	UPPER CONFID. LIMIT	STANDARD ERROR OF COEFF.EST.
1	123.70	.10178E-01	0.46070E-03	0.19895E-01	0.58293E-02
2	146.78	-.56197E-01	-0.66238E-01	-0.46156E-01	0.60235E-02
3	134.09	141.08	139.04	143.12	1.2251

ADJUSTED SUMS OF SQUARES	PARTIAL F TEST VALUE	P(EXCEEDING F UNDER HYP.I)
50.726	3.0483	0.85208E-01
1448.4	87.041	0.00000E+00
0.00000E+00	0.00000E+00	0.00000E+00

Fig. 14: Summary of multiple regression analysis for different parameters

a) geopotential anomaly 25/1500 dBar

SOURCE OF VARIATION	DEGREES OF FREEDOM	SUMS OF SQUARES	MEAN SQUARES
REGRESSION	2.00000	826.61093	413.30547
RESIDUAL	72.00000	560.75687	7.78829
TOTAL	74.00000	1387.36780	

F-VALUE FOR NULL HYPOTHESIS TEST
(ALL REGRESSION PARAMETER ZERO)

53.06755

PROBABILITY OF EXCEEDING F UNDER ASSUMPTION OF THE NULL HYPOTHESIS

0.00000

PERCENTAGE OF VARIATION EXPLAINED	STAND. DEVIATION OF RESIDUALS	STD. DEV. AS PERCENTAGE OF RESPONSE MEAN
59.58124	2.79075	3.33331

REGRESSION COEFFICIENT INTERFERENCES

DIGITS OF ACCURACY FOR REGRESSION COEFF. ESTIMATES

4.0

VARIABLE NUMBER I	MEAN	REGRESSION COEFFICIENT	LOWER CONFID. LIMIT	UPPER CONFID. LIMIT	STANDARD ERROR OF COEFF.EST.
1	124.00	-.64742E-03	-0.70556E-02	0.57608E-02	0.38458E-02
2	146.87	-.42115E-01	-0.48927E-01	-0.35303E-01	0.40880E-02
3	83.723	89.989	88.596	91.381	0.83547

ADJUSTED SUMS OF SQUARES	PARTIAL F TEST VALUE	P(EXCEEDING F UNDER HYP.I)
0.22072	0.28340E-01	0.86678
826.59	106.13	0.00000E+00
0.00000E+00	0.00000E+00	0.00000E+00

Fig. 14: Summary of multiple regression analysis for different parameters

b) geopotential anomaly 25/700 dBar

SOURCE OF VARIATION	DEGREES OF FREEDOM	SUMS OF SQUARES	MEAN SQUARES
REGRESSION	2.00000	0.78883	0.39442
RESIDUAL	75.00000	0.65849	0.00878
TOTAL	77.00000	1.44733	

F-VALUE FOR NULL HYPOTHESIS TEST (ALL REGRESSION PARAMETER ZERO)

44.92256

PROBABILITY OF EXCEEDING F UNDER ASSUMPTION OF THE NULL HYPOTHESIS

0.00000

PERCENTAGE OF VARIATION EXPLAINED	STAND. DEVIATION OF RESIDUALS	STD. DEV. AS PERCENTAGE OF RESPONSE MEAN
54.50275	0.09370	0.34918

REGRESSION COEFFICIENT INTERFERENCES

DIGITS OF ACCURACY FOR REGRESSION COEFF. ESTIMATES

4.0

VARIABLE NUMBER I	MEAN	REGRESSION COEFFICIENT	LOWER CONFID. LIMIT	UPPER CONFID. LIMIT	STANDARD ERRO OF COEFF.EST.
1	126.15	-.10878E-03	-0.31295E-03	0.95382E-04	0.12259E-03
2	145.06	.12822E-02	0.10561E-02	0.15082E-02	0.13573E-03
3	26.834	26.662	26.617	26.707	0.27067E-01

ADJUSTED SUMS OF SQUARES	PARTIAL F TEST VALUE	P(EXCEEDING F UNDER HYP.I)
0.69136E-02	0.78743	0.37772
0.78347	89.234	0.00000E+00
0.00000E+00	0.00000E+00	0.00000E+00

Fig. 14: Summary of multiple regression analysis for different parameters

c) potential density at 250 dBar

SOURCE OF VARIATION	DEGREES OF FREEDOM	SUMS OF SQUARES	MEAN SQUARES
REGRESSION	2.00000	24.68738	12.34369
RESIDUAL	75.00000	12.03227	0.16043
TOTAL	77.00000	36.71965	

F-VALUE FOR NULL HYPOTHESIS TEST
(ALL REGRESSION PARAMETER ZERO)

76.94112

PROBABILITY OF EXCEEDING F UNDER ASSUMPTION OF THE NULL HYPOTHESIS

0.00000

PERCENTAGE OF VARIATION EXPLAINED	STAND. DEVIATION OF RESIDUALS	STD. DEV. AS PERCENTAGE OF RESPONSE MEAN
67.23206	0.40054	2.32973

REGRESSION COEFFICIENT INTERFERENCES

DIGITS OF ACCURACY FOR REGRESSION COEFF. ESTIMATES

4.0

VARIABLE NUMBER I	MEAN	REGRESSION COEFFICIENT	LOWER CONFID. LIMIT	UPPER CONFID. LIMIT	STANDARD ERROR OF COEFF.EST.
1	126.15	.92870E-03	0.55968E-04	0.18014E-02	0.52403E-03
2	145.06	-.71346E-02	-0.81009E-02	-0.61683E-02	0.58021E-03
3	17.192	18.110	17.918	18.303	0.11570

ADJUSTED SUMS OF SQUARES	PARTIAL F TEST VALUE	P(EXCEEDING F UNDER HYP.)
0.50388	3.1408	0.80419E-01
24.259	151.21	0.00000E+00
0.00000E+00	0.00000E+00	0.00000E+00

Fig. 14: Summary of multiple regression analysis for different parameters

d) surface temperature

SOURCE OF VARIATION	DEGREES OF FREEDOM	SUMS OF SQUARES	MEAN SQUARES
REGRESSION	2.00000	1.31180	0.65590
RESIDUAL	75.00000	0.73615	0.00982
TOTAL	77.00000	2.04795	

F-VALUE FOR NULL HYPOTHESIS TEST
(ALL REGRESSION PARAMETER ZERO)

66.82385

PROBABILITY OF EXCEEDING F UNDER ASSUMPTION OF THE NULL HYPOTHESIS

0.00000

PERCENTAGE OF VARIATION EXPLAINED	STAND. DEVIATION OF RESIDUALS	STD. DEV. AS PERCENTAGE OF RESPONSE MEAN
64.05424	0.09907	0.27178

REGRESSION COEFFICIENT INTERFERENCES

DIGITS OF ACCURACY FOR REGRESSION COEFF. ESTIMATES

4.0

VARIABLE NUMBER I	MEAN	REGRESSION COEFFICIENT	LOWER CONFID. LIMIT	UPPER CONFID. LIMIT	STANDARD ERROR OF COEFF.EST.
1	126.15	.47663E-03	0.26076E-03	0.69250E-03	0.12962E-03
2	145.06	-.15787E-02	-0.18177E-02	-0.13397E-02	0.14351E-03
3	36.453	36.622	36.575	36.670	0.28619E-01

ADJUSTED SUMS OF SQUARES	PARTIAL F TEST VALUE	P(EXCEEDING F UNDER HYP.I)
0.13272	13.522	0.44172E-03
1.1878	121.01	0.00000E+00
0.00000E+00	0.00000E+00	0.00000E+00

Fig. 14: Summary of multiple regression analysis for different parameters

e) surface salinity

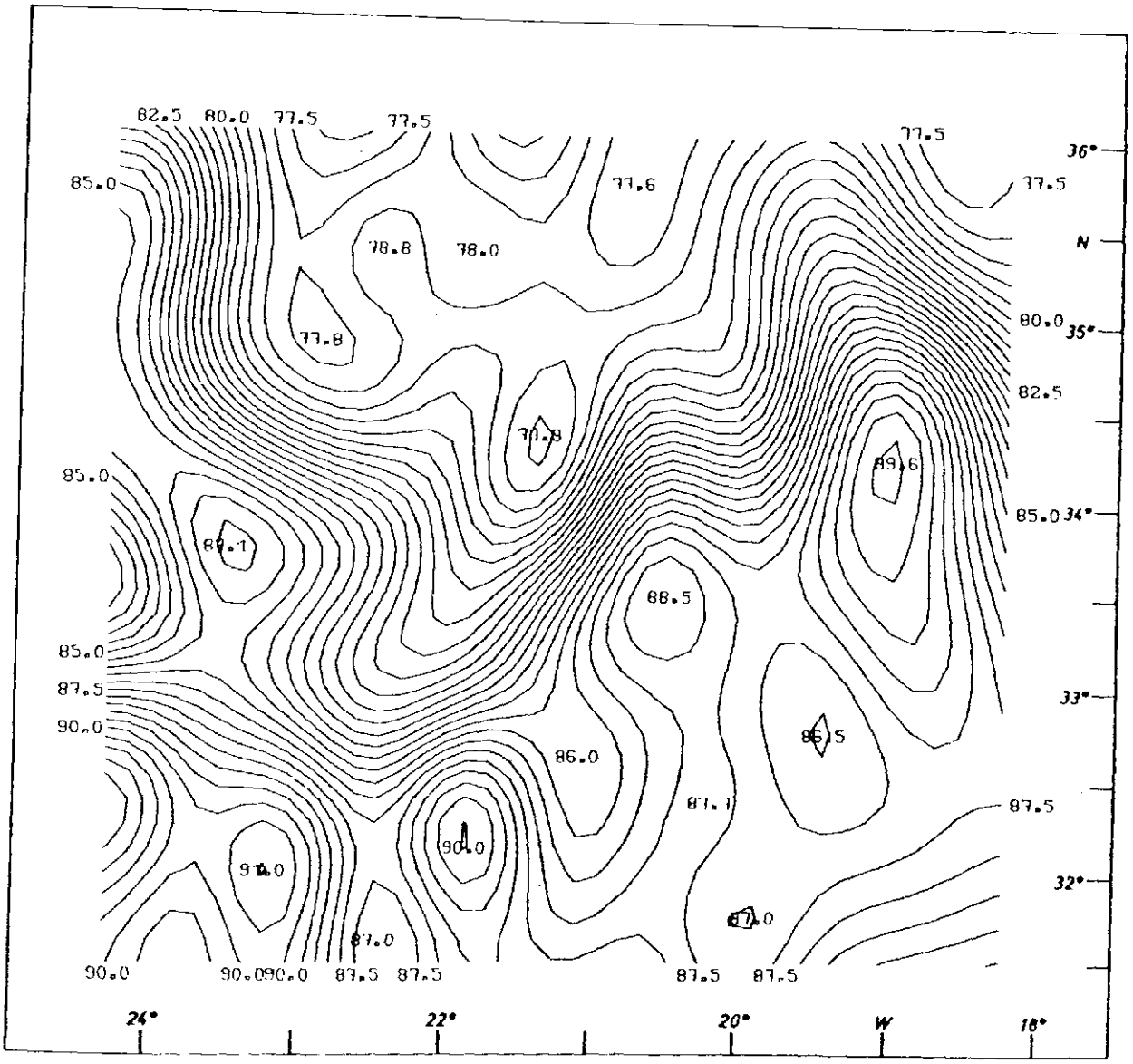

Fig. 15: a) Objective analysis of the geopotential anomaly field 25/700 dBar

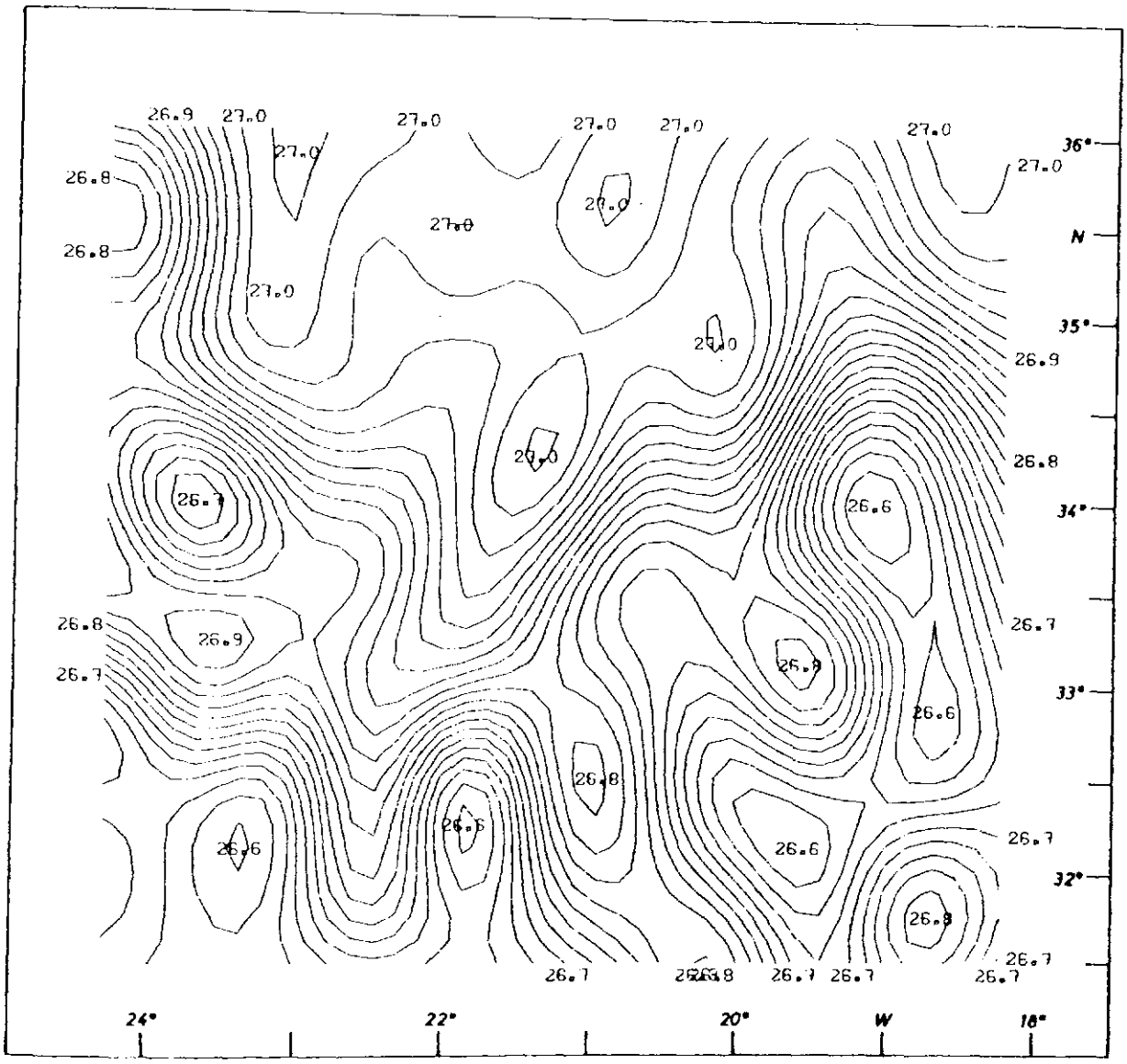

Fig. 15: b) Objective analysis of the potential density field at 250 dBar

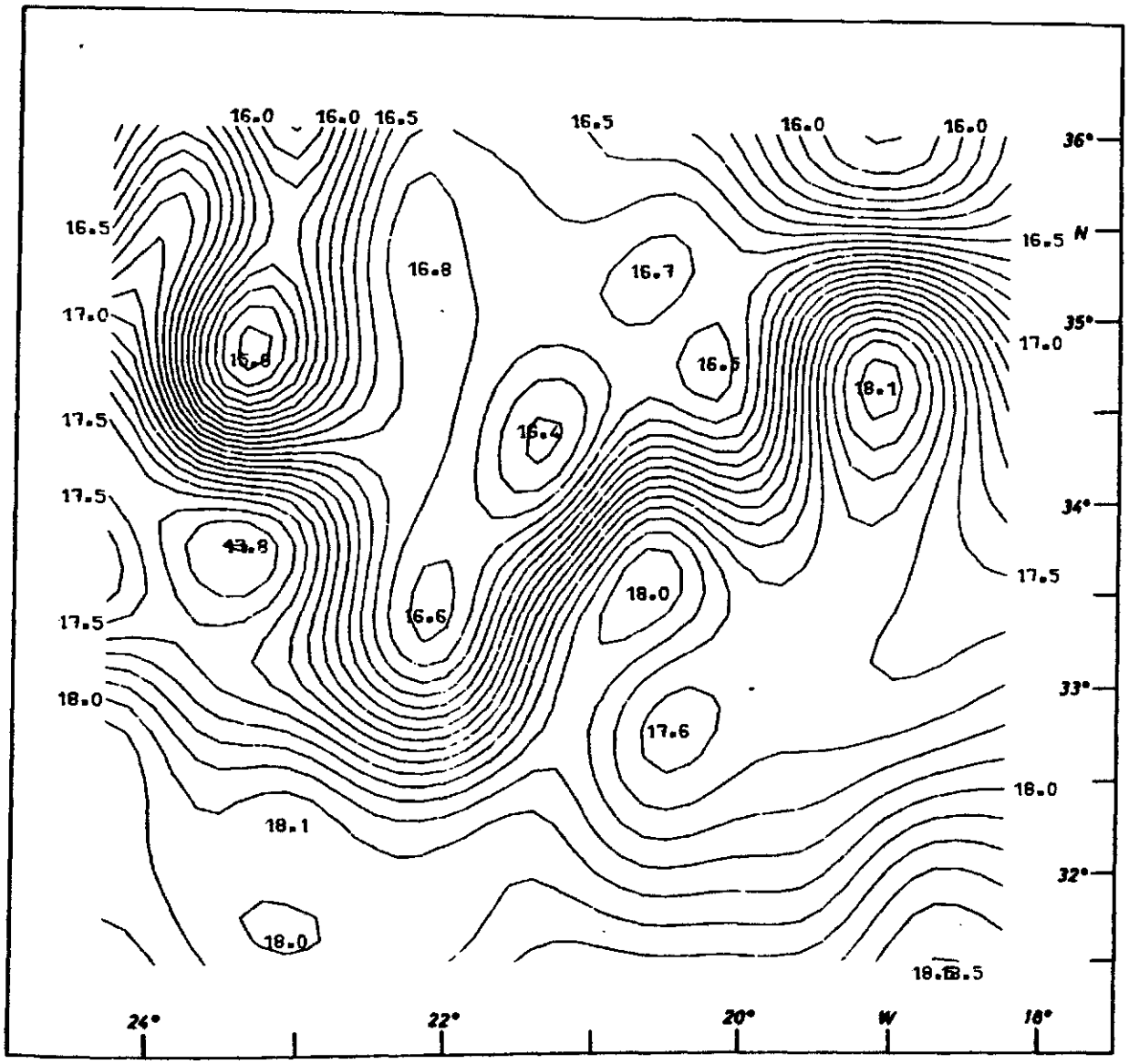

Fig. 15: c) Objective analysis of the 25 dBar temperature field

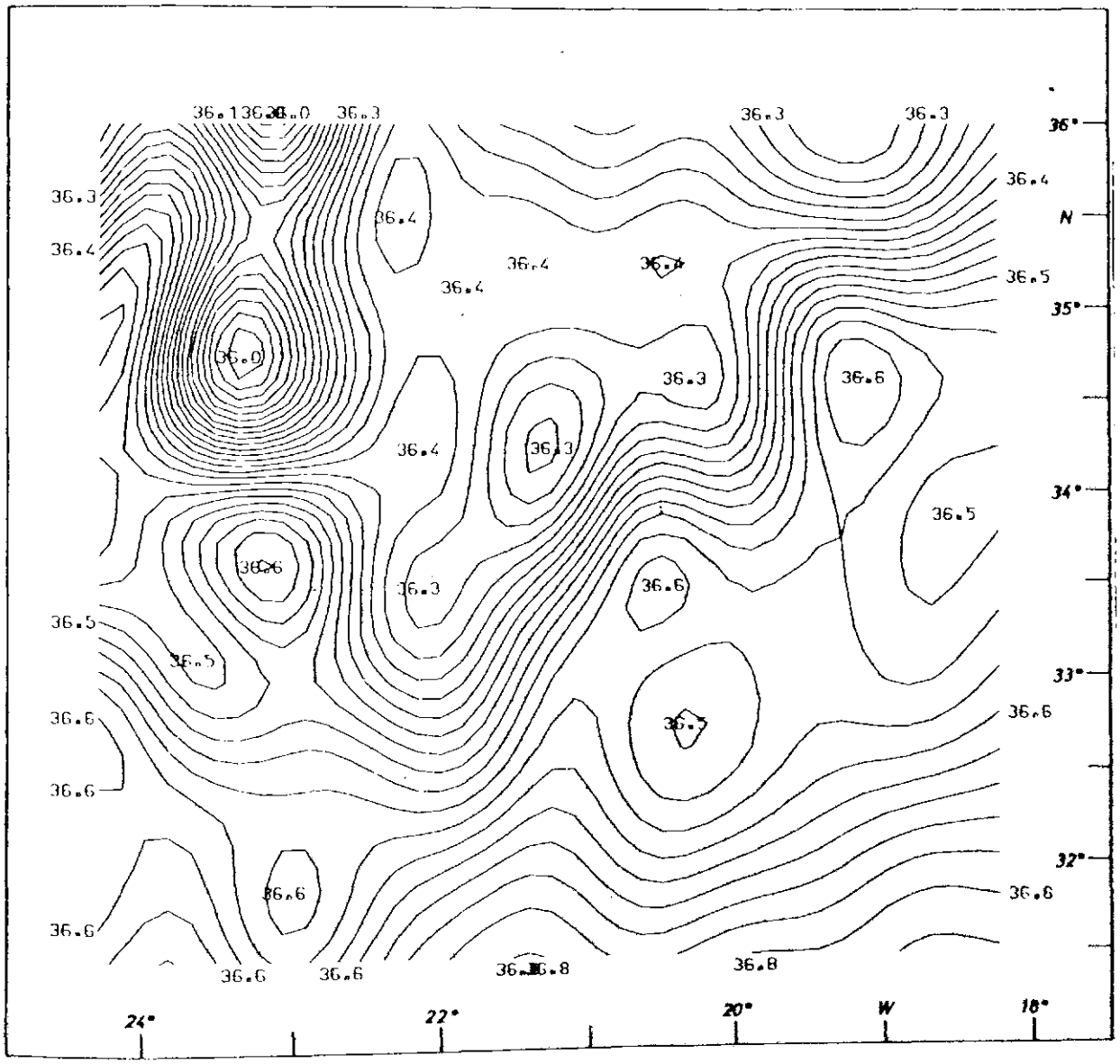

Fig. 15: d) Objective analysis of the 25 dBar salinity field